EUROPEAN ORGANIZATION FOR NUCLEAR RESEARCH

CERN-EP/84-39
March 26, 1984

A STUDY OF HIGH TRANSVERSE MOMENTUM ELECTRONS PRODUCED IN $\bar{p}p$ COLLISIONS AT 540 GeV

The UA2 Collaboration

Bern[1] - CERN[2] - Copenhagen (NBI)[3] - Orsay (LAL)[4] - Pavia[5] - Saclay (CEN)[6] Collaboration

P. Bagnaia[2], M. Banner[6], R. Battiston[a], Ph. Bloch[6], F.Bonaudi[2], K. Borer[1], M. Borghini[2], J. Bürger[2,b], P. Cenci[a], J.-C. Chollet[4], A.G. Clark[2], C. Conta[5],P. Darriulat[2], L. Di Lella[2], J. Dines-Hansen[3], P.A. Dorsaz[2,c], R. Engelmann[2,d], L. Fayard[4], M. Fraternali[5], D. Froidevaux[4], G. Fumagalli[5], J.-M. Gaillard[4], O. Gildemeister[2], V.G. Goggi[5], C. Gössling[2], B. Hahn[1], H. Hänni[1], J.R. Hansen[2], P. Hansen[2,3], N. Harnew[2], T. Himel[2,e], V. Hungerbühler[2,f], P. Jenni[2], O. Kofoed-Hansen[3], E. Lançon[6], M. Livan[2,5], S. Loucatos[6], B. Madsen[3], P. Mani[1], B. Mansoulié[6], G.C. Mantovani[a], L. Mapelli[2,g], B. Merkel[4], R. Möllerud[3], B. Nilsson[3], C. Onions[2], G. Parrour[4], F. Pastore[5], H. Plothow-Besch[2], M. Polverel[6], J.-P. Repellin[4], A. Rimoldi[5], A. Rothenberg[2], A. Roussarie[6], G. Sauvage[4], J. Schacher[1], J.L. Siegrist[2,h], G. Stimpfl[2], F. Stocker[1], M. Swartz[2], J. Teiger[6], S. Tovey[2,i], V. Vercesi[5], A.R. Weidberg[2], H. Zaccone[6], J.A. Zakrzewski[2,j] and W. Zeller[1].

(Submitted to Zeitschrift für Physik C)

ABSTRACT

The production of electrons with very high transverse momentum has been studied in the UA2 experiment at the CERN $\bar{p}p$ collider ($\sqrt{s}$ = 540 GeV). From a sample of events containing an electron candidate with $p_T > 15$ GeV/c, we extract a clear signal resulting from the production of the charged intermediate vector boson $W^{\pm}$, which subsequently decays into an electron and a neutrino. We study the W production and decay properties. Furthermore, we refine our results on the production and decay of the neutral vector boson Z^0. Finally, we compare the experimental results to the predictions of the standard model of the unified electro-weak theory.

---

1. Laboratorium für Hochenergiephysik, Universität Bern, Sidlerstrasse 5, Bern, Switzerland.
2. CERN, 1211 Geneva 23, Switzerland.
3. Niels Bohr Institute, Blegdamsvej 17, Copenhagen, Denmark.
4. Laboratoire de l'Accélérateur Linéaire, Université de Paris-Sud, Orsay, France.
5. Dipartimento di Fisica Nucleare e Teorica, Università di Pavia and INFN, Sezione di Pavia, Via Bassi 6, Pavia, Italy.
6. Centre d'Etudes Nucléaires de Saclay, France.

a) Gruppo INFN del Dipartimento di Fisica dell'Università di Perugia, Italy.
b) On leave from DESY, Hamburg, FRG.
c) Now at the University of Geneva, Geneva, Switzerland.
d) On leave from State University of New York, Stony Brook, NY, USA.
e) Now at SLAC, Stanford University, Stanford, USA.
f) Now at LeCroy Research Systems, Geneva, Switzerland.
g) On leave from INFN, Pavia, Italy.
h) Now at Dept. of Physics, University of California, Berkeley, USA.
i) On leave of absence from the University of Melbourne, Australia.
j) On leave from Institute of Physics, University of Warsaw, Poland.

1. INTRODUCTION

We have recently reported [1] the observation of single isolated electrons with high transverse momentum (p_T) in events with missing transverse energy at the CERN $\bar{p}p$ collider ($\sqrt{s}$ = 540 GeV), from a data sample corresponding to a total integrated luminosity of 15 nb^{-1} collected during the Autumn of 1982. This observation was consistent with the expectations from the process

$$\begin{aligned} \bar{p} + p \rightarrow\ & W^{\pm} + \text{anything} \\ & \rightarrow e^{\pm} + \nu\ (\bar{\nu}) \end{aligned} \qquad (1)$$

where $W^{\pm}$ is the charged Intermediate Vector Boson (IVB) postulated by the unified electroweak theory [2].

More recently, we have also reported [3] the observation of eight events which were interpreted in terms of the reaction

$$\begin{aligned} \bar{p} + p \rightarrow\ & Z^0 + \text{anything} \\ & \rightarrow e^+ + e^- \quad \text{or} \quad e^+ + e^- + \gamma \end{aligned} \qquad (2)$$

where Z^0 is the neutral IVB. These events were found in a data sample corresponding to a total integrated luminosity of 131 nb^{-1} collected during the 1982 and 1983 periods of collider operation.

We report here the final results from a search for electrons with $p_T > 15$ GeV/c performed on the entire data sample available so far. The main motivation for this study is a comparison with improved statistics between the experimental data and the expectations from reactions (1) and (2) in the framework of the standard model [4].

Before selecting the final sample of events which can be interpreted in terms of reaction (1), we present a general discussion on the topology of all events which contain a high-p_T electron candidate, in particular with regard to the possible presence of hadronic jets in some of these events. Since two-jet events are the main source of background to a signal of high-p_T electrons, a study of the event

configuration is useful, as we shall see in Section 6, to provide a reliable estimate of the expected background.

Preliminary results from the study reported in this paper have been presented elsewhere [5,6].

2. THE DETECTOR

The experimental apparatus, shown in Fig. 1, has been described in detail elsewhere [7]. At the centre of the apparatus a system of cylindrical chambers (the vertex detector [8]) measures charged particle trajectories in a region without magnetic field. The vertex detector consists of : a) four multi-wire proportional chambers, C_1 to C_4, with wires parallel to the beam axis and cathode strips at ±45° to the wires ; b) a scintillation counter hodoscope (VH), consisting of 24 elements in a barrel-like arrangement, located after chamber C_2 ; c) two drift chambers with measurement of the charge division on the wires. The drift chambers are used to obtain both tracking information (from a total of 12 wires per track) and to provide a measurement of the most likely ionisation I_0 associated with each track. From the reconstructed tracks the position of the event vertex is determined with a precision of ±1 mm in all directions.

The polar angle interval $40° < \theta < 140°$ is covered over the full azimuth by the central calorimeter [9], which surrounds the vertex detector. This calorimeter is segmented into 240 independent cells, each covering 10° in θ and 15° in ϕ and built in a tower structure pointing to the centre of the interaction region. Each cell is segmented longitudinally into a 17 radiation length thick electromagnetic compartment (lead-scintillator) followed by two hadronic compartments (iron-scintillator) of ~ 2 absorption lengths each. The light from each compartment is channeled to two photomultipliers (PMs) by means of wave-length shifting BBQ-doped plexiglass plates located on opposite sides of the cell.

In the angular region covered by the central calorimeter a cylindrical tungsten converter, 1.5 radiation lengths thick, is located just after the vertex detector. This converter is followed by a cylindrical multi-wire proportional chamber, named C_5 in Fig. 1, similar in construction and operation to chambers C_1 to C_4 but equipped also with measurement of the charge division on the wires. This device, referred to in the following as preshower counter, localises electromagnetic showers initiated in the tungsten with a precision of ±3 mm, as verified using test-beam electrons.

For the first 15 nb^{-1} of integrated luminosity, collected during the autumn of 1982, the azimuthal coverage of the central calorimeter was only 300°. The remaining interval (±30° around the horizontal plane) was covered by a magnetic spectrometer which included a lead-glass array to measure charged and neutral particle production [10,11].

The two forward regions ($20° < \theta < 37.5°$ and $142.5° < \theta < 160°$) are each equipped with twelve coils equally spaced in azimuth (see Fig. 1), which generate a toroidal magnetic field with an average bending power of 0.38 T·m. Each sector (see Fig. 2) is instrumented with :

a) three drift chambers [12] located after the magnetic field region. Each chamber contains three planes, with wires at -7°, 0° and +7° with respect to the magnetic field direction. These chambers are used in association with the event vertex to measure charged particle momenta. The momentum resolution is $\Delta(1/p) \approx 1\%$ $(GeV/c)^{-1}$.

b) a 1.4 radiation length thick lead-iron converter, followed by a preshower counter which consists of two pairs of layers of 20 mm diameter proportional tubes (MTPC), staggered by a tube radius and equipped with pulse height measurement [13]. There is an angle of 77° between the tubes of the two pairs of layers, with the tubes of the first one being parallel to the magnetic field direction. This device localises electromagnetic showers initiated in the converter with a precision of ±6 mm.

c) an electromagnetic calorimeter consisting of lead-scintillator counters assembled in ten independent cells, each covering 15° in ϕ and 3.5° in θ. Each cell is subdivided into two independent longitudinal sections 24 and 6 radiation lengths thick, the latter providing rejection against hadrons. The light from each section is collected by two wave-length shifting BBQ-doped light guides on opposite sides of the cell.

All calorimeters have been calibrated in a 10 GeV beam from the CERN PS, using incident electrons, hadrons and muons. The stability of the calibration has since been monitored using a light flasher system, a Co^{60} source and a measurement of the average energy flow into each module for unbiased $\bar{p}p$ collisions [9]. A further check on the calibration stability has been performed in December 1982 with the recalibration of 80 cells of the central calorimeter in a 10 GeV beam from the CERN PS. The systematic uncertainty in the energy calibration of the electromagnetic calorimeters for the data discussed in this paper amounts to an average value of ±1.5%. The cell-to-cell calibration uncertainty has a distribution with a r.m.s. deviation of 2.2% with respect to its mean.

The response of the calorimeters to electrons, and to single and multi-hadrons, has been measured at the CERN PS and SPS using beams from 1 to 70 GeV. In particular, both longitudinal and transverse shower developments have been studied, as well as the effect of particles impinging near the cell boundaries. The energy resolution for electrons is measured to be $\sigma_E/E = 0.14/\sqrt{E}$ [9] in the central calorimeter and $0.17/\sqrt{E}$ in the forward ones (E in GeV).

3. DATA TAKING

In order to implement a trigger sensitive to electrons of high transverse momentum, the PM gains in all calorimeters were adjusted so that their signals were proportional to the transverse energy.

Because of the cell dimensions, electromagnetic showers initiated by electrons may be shared among adjacent cells. Trigger thresholds were applied, therefore, to linear sums of signals from matrices of 2 × 2 cells, rather than to individual cells. In the central calorimeter, all possible 2 × 2 matrices were considered ; in the two forward ones, we included only those consisting of cells belonging to the same sector.

A signal was generated whenever the linear sum from at least one such matrix exceeded a threshold which was typically set at 8 GeV. To suppress background from sources other than $\bar{p}p$ collisions, we required a coincidence with two signals obtained from scintillator hodoscopes covering the polar angle interval 0.47° - 2.84° with respect to the beams on both sides of the collision region. These hodoscopes, which were part of an experiment to measure the $\bar{p}p$ total cross-section [14], gave a coincidence signal in more than 98% of all non-diffractive $\bar{p}p$ collisions.

Approximately 7×10^5 triggers were recorded during the 1982 and 1983 runs, corresponding to an integrated luminosity $\mathscr{L} = 131\ nb^{-1}$.

4. DATA ANALYSIS

High-p_T electrons are identified by requiring that the event satisfies the following main criteria :

a) the presence of a localised cluster of energy deposition in the first compartment of the calorimeters, with only a small energy leakage in the hadronic compartment.

b) the presence of a reconstructed charged particle track which points to the energy cluster. The pattern of energy deposition must agree with that expected from an isolated electron incident along the track direction.

c) the presence of a hit in the preshower counter, with an associated pulse height larger than that of a minimum ionising particle (m.i.p.). The distance of the hit from the track must be consistent with the space resolution of the counter itself. Both these features are a distinctive feature of the early shower developed in the converter by a high- energy electron.

In practice, because the central and forward detectors are not identical, these criteria are applied in different ways in the two regions.

In the central calorimeter, energy clusters are obtained by joining all electromagnetic cells which share a common side and contain at least 0.5 GeV. A halo contribution from the cells having at least one side in common with a cluster cell is also included. The cluster energy E_{cl} is defined as $E_{cl} = E_{em} + E_{had}$, where E_{em} is the sum of the energies deposited in the electromagnetic compartments of the cluster cells and E_{had} is the corresponding sum for the hadronic compartments. The condition that the showers have only a small energy leakage in the hadronic compartments of the calorimeters is applied by requiring that the ratio $H = E_{had}/E_{cl}$ does not exceed a value H_o (see Table Ia), which has been determined using test beams.

Cluster sizes R_θ, R_ϕ are calculated from the cluster centroid and from the values of the angles θ and ϕ at the cell centres, weighted by their energy depositions. The conditions R_θ, R_ϕ < 0.5 cell sizes are required to ensure that the cluster size is compatible with that expected from an electron.

It is then required that a charged particle track, reconstructed in the vertex detector, points to the energy cluster. The distance Δ between the track impact point on the calorimeter and the cluster centroid, defined as $\Delta = \sqrt{(\Delta\theta/10°)^2 + (\Delta\phi/15°)^2}$, must be less than 1. We also compare the energy distribution observed in the 3 × 3 cell matrix centred on the impact cell to that expected for an electron incident along the track, as measured with electron test beams. The pulse height ratio between the two PMs of the impact cell is also taken into account in this comparison, as well as the observed hadronic leakage. From the expected and observed quantities and their estimated errors, we define a χ^2 and we require that its probability $P(\chi^2)$ exceeds a given value P_0 (see Table I). We note that, because most distributions have non-gaussian tails, $P(\chi^2)$ is not a standard χ^2-probability and it must rather be considered as a quality factor.

We finally require the observation of a hit in the preshower counter C_5, whose associated pulse height Q_5 must exceed ~3 m.i.p., and whose distance d from the track, as measured on the C_5 surface, must be less than d_0 (see Table Ia).

In the two forward calorimeters, where the cell is far from the interaction point and its size is much larger than the lateral extension of an electromagnetic shower, the cluster must consist of one or two adjacent cells depending on the impact point of the track reconstructed in the drift chambers. These cells are required to have the same azimuth because there is a small dead region between cells at different azimuths which does not allow clustering across it. We also require that the energy sum of cells adjacent to the cluster and of additional charged particles hitting either the cluster or the adjacent cells (as determined from their momenta under the assumption of zero mass) does not exceed 5% of the cluster energy. The condition that the shower has

only a small energy leakage E_{leak} in the second compartment is applied by requiring that the ratio E_{leak}/E_{em} between the energy depositions in the two compartments does not exceed 0.02 (0.03 if the cluster consists of two adjacent cells).

The information from the forward preshower counter is used to require that a signal above a threshold $Q_0 \approx 6$ m.i.p. is observed in each coordinate plane. The signal position along the magnetic field direction must be within 10 cm of the impact point on the calorimeter, as determined from the pulse height ratio between the two PMs of the cluster cell with the higher energy deposition. We also require that the track impact point on the preshower counter is less than 2 cm away from the position of the preshower signal in both directions. Finally, we require that the charged particle momentum p as measured in the spectrometer, and the energy deposition in the calorimeter agree within errors (see Table Ib).

In both the central and forward calorimeters, a small correction is applied to the measured energy value as a function of the track impact point and angle. The form of this correction has been determined experimentally with electron test beams.

It should be noted that some of the selection criteria just described are satisfied only by electrons which are not accompanied by other high-p_T hadrons hitting the same calorimeter cells as the electron. While these criteria prevent the detection of high-p_T electrons which are contained in a jet of high-p_T particles, they strongly reject fake electrons whose main source is represented by jets consisting mostly of high-p_T photons from π^0 decay. In order to remove electrons from photon conversion in the detector material, we require that the track coordinates are found in at least one of the two innermost chambers of the vertex detector (C_1 or C_2). Furthermore, in the forward detectors we reject the event if we oberve another particle of opposite charge sign produced with an angular separation smaller than 30 mr from the electron candidate. To remove multi-photon jets in the central detector, we require that any other signal observed in the preshower counter C_5 within a cone of 10° half-aperture around the track has an

associated charge which is not larger than the charge Q_s associated with the track.

A summary of the electron identification criteria is given in Table I, together with their estimated efficiencies.

The present analysis is concerned only with electrons having $p_T^e > 15$ GeV/c (approximately 8×10^4 triggers). After applying the cuts defined in Table I this sample is reduced to 225 events containing a total of 227 electron candidates, of which 200 are observed in the central detector and 27 in the forward ones. The p_T distribution of these electrons is shown in Fig. 3.

5. TOPOLOGY OF THE EVENTS CONTAINING AN ELECTRON CANDIDATE

The sample of 225 events still contains, in addition to genuine electrons, fake electrons resulting from misidentified high-p_T hadrons or jets of hadrons.

In the case of genuine electrons, because of lepton number conservation the event must contain either another electron of opposite charge (e.g. $Z^0 \rightarrow e^+e^-$) or a neutrino (e.g. $W \rightarrow e\nu$), which are also emitted, in general, with high p_T.

If the electron candidate is not genuine, but results from a misidentified high-p_T hadron or jet of hadrons, we expect another jet of high-p_T hadrons to be present in the same event at an approximately opposite azimuth. Such a configuration is typical of events containing high-p_T hadronic jets [15,16].

In order to examine the topology of these events, we search for high-p_T jets by using the fine segmentation of the calorimeters to group into clusters all adjacent cells containing an energy deposition in excess of 400 MeV. This procedure to identify high-p_T particles or jets of particles has been described in detail elsewhere [9,15,16].

In the forward detectors, however, the calorimeter thickness is equivalent to only 1 absorption length and hadronic showers are not fully contained. In that case we use the calorimeters to measure the energy of electromagnetic showers, and the magnetic spectrometers to measure charged particle momenta [12].

To each cluster we associate a momentum $\vec{p}_{jet}$ with magnitude equal to the cluster energy and directed from the event vertex to the cluster centroid. Most clusters have low transverse momenta, as expected for the soft secondaries associated with the spectator constituents of the incident p and $\bar{p}$. To preferentially select high-p_T particles resulting from the hard collision which produced the electron candidate, we define as a jet any cluster with a transverse momentum in excess of 3 GeV/c. This value removes most of the spectator particles; the probability to observe at least one cluster with $p_T \geq 3$ GeV/c in minimum bias events is measured to be only 15%.

We find that 45 events contain no additional high-p_T cluster, the electron candidate being the only high-p_T particle observed in the detector. The p_T distribution of the electron candidates in these events is shown in Fig. 4a. Such events either contain a neutrino, as in the case of $W \rightarrow e\nu$ decays, or contain other high-p_T particles which have escaped detection because they were emitted outside the detector acceptance. Two-jet events, with one of the jets misidentified as an electron and the other undetected, are expected to contribute to the latter category. In this case the p_T distribution of these fake electrons is expected to show the rapidly falling behaviour typical of the jet p_T spectrum [15,16].

The remaining 180 events contain at least one additional high-p_T cluster. For these events, Fig. 5a shows the distribution of the azimuthal separation $\Delta\phi$ between the momentum vector of the electron candidate, $\vec{p}_e$, and that of the jet with the highest transverse momentum. The peak at $\Delta\phi = 180°$ corresponds to configurations in which the electron candidate is approximately back-to-back in azimuth to a high-p_T jet. We expect these events to be contaminated by two-jet events in which one of the two jets has been misidentified as an electron.

In order to reduce the two-jet background in this sample we consider for each event all the jets whose momenta $\vec{p}_{jet}$ are separated in azimuth from $\vec{p}_e$ by an angle $\Delta\phi > 120°$, and we use these jets to define the quantity

$$\rho_{opp} = -\vec{p}_T^{\,e} \cdot \Sigma\vec{p}_{T,jet}/|\vec{p}_T^{\,e}|^2 \qquad (3)$$

where $\vec{p}_T^{\,e}$ and $\vec{p}_{T,jet}$ are two-dimensional vectors obtained projecting $\vec{p}_e$ and $\vec{p}_{jet}$ on a plane perpendicular to the beams.

The distribution of ρ_{opp} for the 180 events is shown in Fig. 5b. The $p_T^{\,e}$ distribution for the events which have $\rho_{opp} > 0.2$ (a total of 156 events) is shown in Fig. 4b. This sample contains the eight $Z^0 \rightarrow e^+e^-$ (or $e^+e^-\gamma$) events reported in a previous publication [3], for which the higher $p_T^{\,e}$ value is plotted in Fig. 4b, and 148 events consisting of an electron candidate with jet activity at opposite azimuthal angles.

The $p_T^{\,e}$ distribution of the remaining 24 events with $\rho_{opp} < 0.2$ is shown in Fig. 4c. Of these, 16 events have $\rho_{opp} = 0$, which corresponds to no jet activity whatsoever in an azimuthal sector $\pm 60°$ wide opposite to the electron direction.

The numbers of events observed in the three different topologies are given in Table IIa for the central and forward detectors separately.

6. BACKGROUND ESTIMATE TO THE ELECTRON SPECTRA

The results of the previous section suggest that the sample of 148 events with jet activity at azimuthal angles opposite to that of the electron candidates consists mostly of two-jet events in which one of the two jets has been misidentified as an electron.

Evidence for such background is obtained by applying the strict cuts defined in Table Ia to the 135 electrons detected in the central region which are contained in this sample after removing the eight Z^0 events. Only 74 events survive, or 55% of the sample. In the case of genuine electrons the expected fraction would be equal to the ratio of the cut efficiencies, which is 86%.

This argument suggests that most of the 148 electrons are indeed misidentified hadrons, but it does not exclude the presence of genuine electrons in this sample. A discussion of the possible sources of electron-jet events in an azimuthally opposite configuration is beyond the scope of this paper, and, with the exception of W production at high p_T, such events represent a background to the signal if the jet at $\Delta\phi \approx 180^\circ$ to the electron is not detected in the apparatus. For these reasons, in the following analysis these 148 events are taken as a pure background sample. We note that the rate of occurrence of these events is lower than that of inclusive jet production [16] in the same p_T region by a factor of $\sim 3.6 \times 10^4$ for the central detector and $\sim 2.6 \times 10^5$ for the forward ones.

Backgrounds to the two event samples of Fig. 4a and 4c, which consist of electron candidates without and with jets, respectively, are estimated as follows. We consider a sample of events recorded using the trigger described in section 3, in which, however, no energy cluster with $p_T > 15$ GeV/c passes the electron cuts of Table I. In each of these events we take as an electron the energy cluster with $p_T > 15$ GeV/c (if any) having the smallest hadronic energy leakage. These fake electrons are then analysed in exactly the same way as the sample of electron candidates. In particular, they are subdivided into three samples, called A, B and C, respectively, with sample A containing the

events having no additional jets, and samples B and C consisting of events in which the additional jets satisfy the condition $\rho_{opp} > 0.2$ and $\rho_{opp} < 0.2$, respectively (see Eq. 3).

The ratio between the p_T distribution of sample A to that of sample B gives directly the probability that in two-jet events one of the two jets escapes detection because of the incomplete angular coverage of the apparatus. We find that such probability decreases from ~ 10% to ~ 2% when p_T increases from 15 to 25 GeV/c, and it depends only weakly on the production angle of the fake electron.

We assume that the p_T distributions of the samples A, B and C are similar to those of the background events contained in the corresponding electron samples. We can check this assumption for the 148 electron candidates with $\rho_{opp} > 0.2$ which, as mentioned above, are taken as a pure background sample, and we do indeed find that they have the same p_T distribution as the fake electrons of sample B. The background contributions to the 69 electron candidates in the other two topologies (45 with no additional jets and 24 with jets having $\rho_{opp} < 0.2$) are then estimated directly from the p_T distributions of samples A and C, multiplied by a factor equal to the ratio of the total number of electron candidates with $\rho_{opp} > 0.2$ (148 events) to the total number of events in sample B. These background estimates are shown as smooth curves in Fig. 4a and 4c.

7. THE W → ev EVENT SAMPLE

The two event samples of Fig. 4a and 4c are expected to contain electrons from W → ev decay. The combined p_T^e distribution of these 69 electron candidates is shown in Fig. 6a together with the background estimate, which amounts to 21.4 ± 1.3 events in total. There is a clear accumulation of events near $p_T^e \approx 40$ GeV/c, which is a distinctive characteristic of the Jacobian peak expected for W → ev decay. For $p_T^e > 25$ GeV the distribution of Fig. 6a contains 37 events with an estimated background of 1.5 ± 0.1 events.

As a further check that the electron candidates with $p_T^e > 25$ GeV/c are mostly genuine, we apply the strict electron identification criteria to the 30 electron candidates observed in the central detector. A total of 26 events pass these cuts, as expected from the ratio of the cut efficiencies. The p_T^e distribution for the total sample (but using the strict electron identification criteria in the central detector) is shown in Fig. 6b with the corresponding background estimate.

Further evidence that these events consist of genuine electrons is given in Figs. 7a to 7f, which show the distributions of some of the variables used to define the electron identification criteria (see Table I), such as the ratio E_{had}/E_{cl} (or E_{leak}/E_{em} in the forward regions), the distance between the track and the preshower signal, and the charge measured in the preshower counter. All of these distributions are consistent with an electron behaviour. Finally, Fig. 7g shows a comparison between the most likely ionisation I_0 associated with the electron candidate track, as measured by the drift chambers of the vertex detector, and that measured for tracks in minimum bias events. The I_0 distribution of the electron candidates is peaked at a higher I_0 value than that of minimum bias tracks, as expected from the effect of the relativistic rise of the ionisation loss.

The numbers of $W \rightarrow e\nu$ candidates with $p_T^e > 25$ GeV/c observed in the central and forward detectors, respectively, are given in Table IIb together with the corresponding background estimates.

The presence of a neutrino in $W \rightarrow e\nu$ events can be detected by the resulting transverse momentum imbalance. For each event we compute

$$\vec{p}_T^{\,\nu} = \vec{p}_T^{\,W} - \vec{p}_T^{\,e} \qquad (4)$$

where all vectors are projected onto a plane normal to the beams. The W transverse momentum $\vec{p}_T^{\,W}$ can be determined from the momenta of all other particles, or jets of particles, observed in the event in addition to the electron candidate :

$$\vec{p}_T^{\,W} = -\left(\Sigma\, \vec{p}_{T,jet} + \lambda\, \vec{p}_T^{\,sp} \right) \qquad (5)$$

where the sum extends over all observed jets, $\vec{p}_T^{\,sp}$ is the total transverse momentum carried by the system of all other particles not belonging to jets, and λ is a correction factor which takes into account the incomplete detection of the rest of the event ($\lambda = 1$ for an ideal detector). To determine this correction, we use the eight Z^0 events previously reported [3] (see also Section 11 and Table III) and we compare the mean value of p_T^Z which is directly determined from the transverse momenta of the decay products, with that obtained using Eq.(5), $\langle p_T' \rangle$. We find $\lambda = 2.2 \pm 0.5$ in order to obtain $\langle p_T^Z \rangle = \langle p_T' \rangle$. An estimate of the error on $\langle p_T' \rangle$ is given by the r.m.s. of the difference $p_T^Z - p_T'$ for the eight Z^0 events, whose value is 3.0 GeV/c.

Figure 8 shows both the uncorrected and corrected distribution of p_T^W, as obtained using Eq. (5) with $\lambda = 1.0$ and 2.2, respectively, for the 37 $W \rightarrow e\nu$ candidates having $p_T^e > 25$ GeV/c. The corrected mean value of p_T^W is $\langle p_T^W \rangle = 6.9 \pm 1.0$ GeV/c. There are 5 events with $p_T^W > 12$ GeV/c, the highest p_T^W value being 29.6 GeV/c. QCD predictions [17], illustrated by the curve in Fig. 8, are consistent with the observed distribution.

We obtain the neutrino transverse momentum $\vec{p}_T^{\,\nu}$ from Eq. (4) and we define two components p_ξ^ν and p_η^ν parallel and perpendicular to $\vec{p}_T^{\,e}$, respectively. Figure 9a and 9b show all the 69 events of the sample in the (p_T^e, p_ξ^ν) and (p_T^e, p_η^ν) plane, respectively. Most of the events populate the regions $p_\xi^\nu \approx p_T^e$, $p_\eta^\nu \approx 0$ where $W \rightarrow e\nu$ events with small values of p_T^W are expected to fall. There are three events with $p_\eta^\nu > 20$ GeV/c, which are clearly separated from the rest of the population. The only event of these three with $p_T^e > 25$ GeV/c is that having the highest p_T^W in the distribution of Fig. 8. We interpret this event as the production of a high-p_T W recoiling against a jet, followed by the decay $W \rightarrow e\nu$. The other two events are discussed in a separate publication [18].

In the 37 $W \rightarrow e\nu$ candidates having $p_T^e > 25$ GeV/c, we have also studied the system of all other observed particles (the underlying

event), after removal of the electron and the jets (if any). For the events containing no jet we find a structure similar to that of minimum bias events. More precisely, the average charged particle multiplicity measured over the pseudorapidity interval $|\eta| < 2$ is found to be $\langle n_{ch} \rangle = 15.8 \pm 1.9$ to be compared with the value $\langle n_{ch} \rangle = 14.7 \pm 0.2$ measured for a sample of minimum bias events ; and we measure $\langle \Sigma E_T \rangle = 9.7 \pm 1.2$ GeV for the average value of the sum of the energies of all particles other than the electron, while it is $\sim 8.8 \pm 0.2$ GeV in minimum bias events. If we include the $W \rightarrow e\nu$ events containing jets, these values increase to $\langle n_{ch} \rangle = 19.3 \pm 1.9$ and $\langle \Sigma E_T \rangle = 14.1 \pm 1.7$ GeV. We note also that the occurrence of jets in the $W \rightarrow e\nu$ sample is approximately twice as large as in minimum bias events.

8. DETERMINATION OF THE W MASS

A value of the W mass is extracted from the 37 $W \rightarrow e\nu$ candidates with $p_T^e > 25$ GeV/c by comparing their two-dimensional distribution $d^2n/dp_T^e d\theta_e$, where θ_e is the measured electron polar angle, to that expected from $W \rightarrow e\nu$ decay. A Monte Carlo program is used to generate the distribution $d^2n/dp_T^e d\theta_e$ for different values of the W mass M_W. The W longitudinal momentum distribution is obtained using the quark structure functions of the proton with scaling violations, as given by Glück et al [19]. A p_T^W distribution is generated using the shape given in Ref. [17], where we allow the average value $\langle p_T^W \rangle$ to vary in order to take into account uncertainties of QCD predictions. The decay angular distribution is described by the standard V-A coupling and the detector response is taken into account. A fixed value of the W width, $\Gamma_W = 2.7$ GeV/c², is used.

The best fit to the experimental distribution $d^2n/dp_T^e d\theta_e$ gives $M_W = 83.1 \pm 1.9$ GeV/c², where the error includes an uncertainty of ±1 GeV/c² resulting from the effect of varying $\langle p_T^W \rangle$ between 4 and 10 GeV/c in the fit. This uncertainty is added in quadrature to the statistical error.

In addition to the quoted error, we must take into account the systematic uncertainty in the calorimeter energy calibration, which, as already mentioned in Section 2, amounts to an average value of ±1.5%. The error resulting from the cell-to-cell uncertainty (see Section 2) reduces to $2.2\%/\sqrt{37} \approx 0.4\%$ for our event sample, and is added in quadrature to the previously quoted statistical error.

To summarise we quote

$$M_W = 83.1 \pm 1.9 \text{ (stat.)} \pm 1.3 \text{ (syst.) GeV/c}^2 \qquad (6)$$

where we choose to separate the two errors because most of the systematic errors cancel when comparing the experimental values of M_W and M_Z. Within the quoted errors this value agrees with the result of the UA1 experiment [20], $M_W = 80.9 \pm 1.5\text{(stat.)} \pm 2.4\text{(syst.)}$ GeV/c².

9. CHARGE ASYMMETRY

It is known that, as a consequence of the V-A coupling, the W is always produced with full polarisation along the direction of the incident $\bar{p}$ beam, and a distinctive charge asymmetry can be observed in the decay $W \rightarrow e\nu$. In the W rest frame the angular distribution has the form $(1 - q \cos\theta^*)^2$ where q is -1 for electrons and +1 for positrons, and θ^* is the angle between the charged lepton and the direction of the incident protons. However, precisely the same configuration would result from V+A coupling because in this case all helicities change sign. To maintain full generality and to allow for different amounts of V and A coupling we write the angular distribution in the form

$$dn/d(\cos\theta^*) \propto (1-q \cos\theta^*)^2 + 2 q \alpha \cos\theta^* \qquad (7)$$

where α depends on the ratio x between the A and V coupling (time reversal invariance requires x to be real). Under the assumption that x is the same for both $Wq\bar{q}$ and $We\nu$ couplings, α is given by

$$\alpha = [(1-x^2)/(1+x^2)]^2 \qquad (8)$$

which gives $\alpha = 0$ for $|x| = 1$.

In the UA2 detector a determination of the charge sign is only possible in the forward detectors where a magnetic field is present. Since the sensitivity of the data to the exact form of the angular distribution is highest for values of $\cos\theta^*$ close to ± 1, corresponding to small values of p_T^e, we consider all electrons with $p_T^e > 20$ GeV/c that are detected in the forward regions and passing the cuts defined in Table I.

Such a sample contains 8 events with an estimated background of 0.2 events. A comparison between the electron momentum p and the energy E, as measured in the calorimeter, is made in Fig. 10, which shows the position of these events in the plane $(\hat{p}^{-1}, E^{-1})$, where $\hat{p}$ is the product of the electron momentum with the sign of $q \cos\theta_e$ (θ_e being the laboratory angle of the electron with respect to the proton direction). The horizontal error bars in Fig. 10 represent the uncertainty on the measurement of p^{-1}, which is 0.01 $(GeV/c)^{-1}$.

A clear asymmetry is visible in Fig. 10, with all the events lying on one side of the plot. In order to extract a value of x from these data we compute two-dimensional distributions $f^{\pm}(p_T^e, \theta_e)$ for positrons and electrons separately, using Eqs. (7) and (8) and taking into account the W longitudinal motion. To each event we assign a likelihood $Q_i = f^+\eta^+ + f^-\eta^-$, where $\eta^+(\eta^-)$ is the probability density that the observed particle was a positron (an electron) of momentum p, and the functions $f^{\pm}$ are calculated at the observed values of p_T^e and θ_e. The probability densities $\eta^{\pm}$ reflect the uncertainty in the determination of the charge sign resulting from the error in the momentum measurement. Maximizing the likelihood $\Pi_i Q_i$ we obtain $|x| = 1.0^{+0.5}_{-0.3}$ for the ratio between the strengths of the A and V couplings.

We remark that our event sample consists of seven positrons detected in one hemisphere and one electron detected in the opposite hemisphere. The probability to observe no more than one electron in one of the two hemispheres is ~ 7%.

10. CROSS-SECTION FOR INCLUSIVE W PRODUCTION

We obtain the cross-section σ_W^e for the inclusive process $\bar{p} + p \rightarrow W^{\pm} +$ anything followed by the decay $W \rightarrow e\nu$, from the relation

$$N_W^e = \mathcal{L}\sigma_W^e \varepsilon \eta \qquad (9)$$

where N_W^e is the observed number of $W \rightarrow e\nu$ decays, $\mathcal{L}$ is the integrated luminosity, ε is the detector acceptance, which includes the effect of the p_T^e threshold, and η is the overall efficiency of the electron identification criteria averaged over the central and forward detectors (see Table I).

The detector acceptance ε is calculated using Monte Carlo techniques. The effect of the cut $\rho_{opp} < 0.2$ described in Section 5, which rejects electrons in the presence of hadron jets at opposite azimuthal angles, is taken into account by generating events containing $W \rightarrow e\nu$ decays and jets by means of the ISAJET program [21]. The value so obtained is $\varepsilon = 0.60 \pm 0.01$.

We use all 37 events with $p_T^e > 25$ GeV/c, for which $\eta = 0.77 \pm 0.05$. This sample is contaminated by misidentified electrons (1.5 events), by electrons from $Z^0 \rightarrow e^+e^-$ decay with one electron undetected, and from $W \rightarrow \tau\nu_\tau$ followed by $\tau \rightarrow e\nu_e\nu_\tau$.

The Z^0 contribution is estimated by a Monte Carlo technique. If we normalise the result to the total number of $Z^0 \rightarrow e^+e^-$ events observed in this experiment (eight events, as reported in Ref. 3), we obtain 2.5 ± 0.9 events.

The contribution from the $W \rightarrow \tau\nu_\tau$, $\tau \rightarrow e\nu_e\nu_\tau$ decay chain to the remaining 33 ± 6.2 events is taken into account by writing $N_W^e = 33/(1 + \varepsilon_\tau B_\tau/\varepsilon)$ where ε_τ is the detector acceptance for electrons from the $W \rightarrow \tau \rightarrow e$ decay chain, and $B_\tau = 0.17$ is the branching ratio for the decay $\tau \rightarrow e\nu_e\nu_\tau$ [22]. From the value $\varepsilon_\tau = 0.10 \pm 0.01$, which we obtain by Monte Carlo techniques, we derive the value $N_W^e = 32.1 \pm 6.0$ for the number of $W \rightarrow e\nu$ decays in our sample.

The sum of all contributions to the 37 events with $p_T^e > 25$ GeV/c is shown as a dashed curve in Fig. 6a. It should be noted that electrons from $Z^0 \rightarrow e^+e^-$ and $W \rightarrow \tau \rightarrow e$ decays in this sample have a rather flat p_T^e distribution and their effect on the determination of the W mass (see Section 8) is negligible.

From the value of the total integrated luminosity, $\mathscr{L} = 131$ nb^{-1}, we obtain

$$\sigma_W^e = 0.53 \pm 0.10(\text{stat.}) \pm 0.10(\text{syst.}) \text{ nb} \qquad (10)$$

where the systematic error reflects a ±20% uncertainty in the knowledge of $\mathscr{L}$. This value is in agreement with QCD predictions [17,23] and with the results of the UA1 experiment [20].

11. THE DECAY $Z^0 \rightarrow e^+e^-$

The observation in this experiment of seven $Z^0 \rightarrow e^+e^-$ decays and one $Z^0 \rightarrow e^+e^-\gamma$ decay has already been reported [3]. Following a recent recalibration of the calorimeters, the invariant mass values of these events and their errors have been slightly modified (see Table III). The updated value of the Z^0 mass based on the weighted average of events A, B, C and E is

$$M_Z = 92.7 \pm 1.7(\text{stat.}) \pm 1.4(\text{syst.}) \text{ GeV/c}^2 \qquad (11)$$

We recall that this value is obtained using only the four events for which the energy of both electrons (and that of the photon in the $e^+e^-\gamma$ event) is unambiguously determined. Within errors, this result agrees with the Z^0 mass value determined in the UA1 experiment, $M_Z = 95.6 \pm 1.4(\text{stat.}) \pm 2.9(\text{syst.})$ GeV/c^2 [24].

In order to extract an estimate of the Z^0 width, Γ_Z, from these four events, we first note that the r.m.s. deviation of the four mass values

from the value of M_Z given by Eq. (11) is 2.0 GeV/c^2, which is almost the same as the weighted average of the errors σ = 2.1 GeV/c^2. To obtain an upper limit to Γ_Z, we use a Monte Carlo program which generates a large number of event samples, each consisting of four $Z^0 \rightarrow e^+e^-$ decays, according to a Breit-Wigner shape and taking into account the energy resolution of the detector. As an estimate of the upper limit to Γ_Z at the 90% (95%) confidence level, we use the value which gives an r.m.s. of less than 2.0 GeV/c^2 in 10% (5%) of the event samples. This value is $\Gamma_Z < 6.5 \pm 0.6$ GeV/c^2 ($\Gamma_Z < 9.9 \pm 0.7$ GeV/c^2) at the 90% (95%) confidence level. The errors given here are systematic errors resulting from the possible variation of the r.m.s. with different event weighting, and from the variation of Γ_Z as a function of the σ value used. They reflect the possible uncertainty in estimating the errors in the energy measurements. It should be noted that if the mass errors have been overestimated, the upper limit to Γ_Z would decrease.

A larger statistical sample and smaller systematic errors are clearly needed before reaching a definitive conclusion on the value of Γ_Z from this technique.

Within the standard model , this upper limit can be related to the number of additional light neutrinos ΔN_ν. We find $\Delta N_\nu < 22 \pm 3$ ($\Delta N_\nu < 41 \pm 4$) at the 90% (95%) confidence level, assuming $\sin^2\theta_W = 0.22$ and a value of the t-quark mass $m_t > M_Z/2$ (we choose this value because it gives the highest upper limit for ΔN_ν).

An independent estimate of Γ_Z can be obtained within the standard model by measuring the ratio $R = \sigma_Z^e/\sigma_W^e$ where σ_Z^e is the cross-section for inclusive Z^0 production followed by the decay $Z^0 \rightarrow e^+e^-$ [26]. We obtain σ_Z^e after corrections which take into account the detector acceptance (57%, as estimated by Monte Carlo techniques) and the efficiency of the electron identification criteria. In this case we use all eight events, for which at least one electron passes all cuts and we find

$$\sigma_Z^e = 0.11 \pm 0.04(\text{stat.}) \pm 0.02(\text{syst.}) \text{ nb} \qquad (12)$$

which is approximately twice as large as the value predicted by QCD [17,25]. For comparison, the UA1 result is [24] $\sigma_Z^e = 0.050 \pm 0.020(\text{stat.}) \pm 0.009(\text{syst.})$ nb.

The error on R is dominated by statistics, because the value of the total integrated luminosity cancels out. We find $R = 0.21 \pm 0.08$ and $R > 0.116$ ($R > 0.098$) at the 90% (95%) confidence level. QCD estimates of the ratio between Z^0 and W production cross-sections [26] provide a relation between R and the ratio Γ_W/Γ_Z :

$$\Gamma_W/\Gamma_Z = (9.3 \pm 0.9)\ R \qquad (13)$$

where the error reflects the uncertainty of the QCD calculations. Using the standard model value of Γ_W, $\Gamma_W = 2.77$ GeV/c² (which corresponds to a t-quark mass $m_t = M_Z/2$) we find $\Gamma_Z < 2.6 \pm 0.3$ GeV/c² ($\Gamma_Z < 3.1 \pm 0.3$ Gev/c²) at the 90% (95%) confidence level.

As before, we can extract upper limits to the number of additional light neutrinos ΔN_ν. We find $\Delta N_\nu \leq 0$ ($\Delta N_\nu < 2$) at the 90% (95%) confidence level. If we decrease the numerical factor in Eq. (13) by its error, these limits become 1 and 4, respectively. Again, a larger statistical sample is clearly needed.

Our result suggests a smaller value of Γ_Z than the standard model prediction, $\Gamma_Z = 2.7$ GeV/c², which would give $R = 0.11$. In this case the probability to find an experimental value $R \geq 0.21$ is 6%. Since we have determined this value by using all the eight Z^0 events, we have considered the possibility that a fraction of these events does not result from $Z^0 \rightarrow e^+e^-$ decay, as suggested by the fact that in three of them one of the two electrons does not pass the cuts of Table I because the pattern of energy deposition in the calorimeter is not consistent with that expected from an electron [3]. Recent measurements performed using test beam electrons of 40 GeV from the SPS impinging on the calorimeter in the same geometrical configuration as the three electrons in the $Z^0 \rightarrow e^+e^-$ events have confirmed this inconsistency. However, in all of these three events the other electron passes all strict cuts, and furthermore, their mass values fall within ± 9 GeV/c² of the Z^0 mass,

with no other event appearing in the e^+e^- invariant mass distribution down to a mass threshold of 50 GeV/c^2. In addition, as mentioned in Ref. 3, the background contamination to the eight events is estimated to be 0.03 events only. For these reasons we retain the interpretation that all of our eight Z^0 events contain an e^+e^- pair.

12. THE DECAY $Z^0 \rightarrow e^+e^-\gamma$

We have reported [3] a $Z^0 \rightarrow e^+e^-\gamma$ event containing a photon with an energy $k = 24$ GeV and an 11 GeV electron clearly separated by an angle $\omega_{lab} = 31°$, excluding, therefore, external bremsstrahlung. In Ref. 3 we estimated that the probability that in a $Z^0 \rightarrow e^+e^-$ decay a photon at least as hard as the observed one is emitted as a result of radiative corrections [27], and the e^+e^- opening angle is equal to, or smaller than the measured one, is $\sim 5 \times 10^{-3}$ per event. This calculation, which was performed in the Z^0 rest frame, should not be considered as an estimate of the probability of such a $Z^0 \rightarrow e^+e^-\gamma$ decay because it does not take into consideration all configurations which are less likely than the observed one (for example, the case $k = 23.5$ GeV, $\omega = 90°$).

There are several possible ways to define the relative likelihood of $Z^0 \rightarrow e^+e^-\gamma$ configurations. For cases of non-collinear $e\gamma$ pairs, the event distribution in the Z^0 rest frame is given by the differential cross-section

$$\frac{d^2\sigma}{dx_1 dx_2} = \sigma_0 \frac{\alpha}{2\pi} \frac{x_1^2 + x_2^2}{(1-x_1)(1-x_2)} \qquad (14)$$

where σ_0 is the total cross-section for $Z^0 \rightarrow e^+e^-$ without radiative corrections, and $x_i = 2E_i/M_Z$, E_i being the electron energies. We say that a configuration is less likely than the observed one if its differential cross-section is smaller than that calculated at the point corresponding to the observed $Z^0 \rightarrow e^+e^-\gamma$ event (see Table IIIb). This definition corresponds to the Neyman-Pearson test [28] which is being used to compare the hypothesis of internal bremsstrahlung to the

hypothesis of a constant differential cross-section. Integrating Eq. (14) over all configurations which are less likely than the observed one we find a probability of 1.4% per event, or 11% to observe at least one such event in a sample of eight. It should be noted that detectable $Z^0 \rightarrow e^+e^-\gamma$ decays can be divided into two classes of configurations, the first consisting of three clearly resolved energy clusters, and the second containing unresolved $e\gamma$ pairs which result in energy clusters inconsistent with an isolated electron. The corresponding probabilities are ~1.0% and ~0.1% per event, respectively. The remaining $Z^0 \rightarrow e^+e^-\gamma$ decays correspond to configurations which are not detectable in the UA2 apparatus.

Another possibility which does not rely on an alternative hypothesis consists in examining the differential cross-section as a function of k and ω. In these variables the following approximation is valid :

$$\frac{d^2\sigma}{dkd\omega} = f(k)g(\omega) \qquad (15)$$

We can use the result [29] that the total probability of events less likely than the observed one is $P = P'(1- \ln P')$ where $P' = 0.005$ is the probability of a $Z^0 \rightarrow e^+e^-\gamma$ decay with a photon at least as hard as the observed one and an $e\gamma$ opening angle at least as large as that observed. This would lead to a total probability $P = 0.03$, or a probability of 21% to observe at least one such event in a sample of eight. This probability is divided roughly equally between the two classes of configurations described earlier.

Finally, we can calculate by means of a simulation program the ratio of the cross-section for producing a detectable $Z^0 \rightarrow e^+e^-\gamma$ event in the UA2 apparatus as a result of internal bremsstrahlung to the total $Z^0 \rightarrow e^+e^-$ and $e^+e^-\gamma$ cross-section. We find a ratio of $1.8 \pm 0.2\%$ for each of the two detectable configurations. This value corresponds to a probability of 13% to detect at least one three-cluster event in a sample of eight, or 25% to observe at least one event inconsistent with a $Z^0 \rightarrow e^+e^-$ hypothesis.

The UA1 collaboration have recently reported the observation of a $Z^0 \rightarrow e^+e^-\gamma$ event [30] which had been previously interpreted as a result of external bremsstrahlung [24]. A similar analysis of the combined sample of 12 $Z^0 \rightarrow e^+e^-$ or $e^+e^-\gamma$ events suggests that the probability to observe two or more $e^+e^-\gamma$ events in this sample is of the order of 5%.

The UA1 collaboration has also reported evidence for a $Z^0 \rightarrow \mu^+\mu^-\gamma$ event [30]. It is not excluded, therefore, that these events may be the manifestation of a new and unexpected decay mode of the Z^0 boson [31]. We remark that there are no means to distinguish between a photon and a low-mass multiphoton system of high transverse momentum in either the UA1 or the UA2 detector.

13. SEARCH FOR THE DECAY $W \rightarrow e\nu\gamma$

Given the interest in unexpected decay modes of the Z^0 we have also looked for events compatible with the decay $W \rightarrow e\nu\gamma$ in the full data sample. In the central detector, we search for events containing an electron candidate with $p_T^e > 8$ GeV/c which passes the cuts of Table Ia, and an additional photon with a momentum k in excess of 8 GeV/c. A photon is defined as an energy cluster which satisfies the same criteria on size and hadronic leakage as an electron, but has no charged particle track pointing to it. If also the photon cluster is seen in the central detector, we require an angular separation $\omega > 30°$ between the cluster centroids in order to resolve the $e\gamma$ pair.

Six events satisfy these conditions. However, none of them survives the additional requirement of a transverse momentum imbalance compatible with the presence of a neutrino having $p_T^\nu > 10$ GeV/c. A Monte Carlo estimate of the number of $W \rightarrow e\nu\gamma$ decays which are expected to satisfy all of these requirements as a result of radiative corrections gives 0.1 event.

In the forward detectors we can identify eγ pairs with very small opening angles by releasing the condition that the electron momentum p and the energy E agree within the measuring errors. In this case, however, we limit our search to electron transverse momenta in excess of 20 GeV/c (as measured in the calorimeter), for which we expect a background contribution of 0.2 events. We find one event which contains a cluster of transverse energy E_T = 41 GeV (E = 86.2 GeV) and a track of 3.6 GeV/c momentum pointing to the cluster and satisfying all other electron identification criteria. Large missing p_T is detected in this event as expected in the case of an associated neutrino. The estimated background for $p_T^e > 35$ GeV/c is 0.01 events. Since the opening angle of this eγ pair is compatible with zero, we also consider the effect of external bremsstrahlung and we obtain a probability of 0.5% per $W \rightarrow e\nu$ decay, or 4.5% to observe one such event in the sample of 9 $W \rightarrow e\nu$ and $e\nu\gamma$ candidates with $p_T^e > 20$ GeV/c detected in the forward detectors.

14. COMPARISON WITH THE SU(2)⊗U(1) MODEL

The IVB mass values predicted in the framework of the standard model taking into account radiative corrections are [32] $M_W = 83.0\,^{+2.9}_{-2.7}$ GeV/c² and $M_Z = 93.8\,^{+2.4}_{-2.2}$ GeV/c². These values are in excellent agreement with our experimental values given in Eq. (6) and (11), respectively.

We can extract a value of $\sin^2\theta_W$ from the definition [33] $\sin^2\theta_W = 1-M_W^2/M_Z^2$, where the systematic errors on the mass scale resulting from the uncertainty in the calorimeter calibration cancel out. We find

$$\sin^2\theta_W = 0.196 \pm 0.035 \qquad (16)$$

in good agreement with the world average result of deep-inelastic neutrino experiments (including radiative corrections), $\sin^2\theta_W = 0.217 \pm 0.014$ (34).

We can extract a more precise value of $\sin^2\theta_W$ from the relation $M_W = A/\sin\theta_W$, where the numerical value $A = 38.65 \pm 0.04$ GeV/c² is obtained taking into account radiative corrections [32]. In this case we find

$$\sin^2\theta_W = 0.216 \pm 0.010(\text{stat.}) \pm 0.007(\text{syst.}) \qquad (17)$$

A test of the standard model is provided by the relationship $\rho = M_W^2/[M_Z^2(1-A^2/M_W^2)]$ which should be equal to 1 for the minimal Higgs structure. We find

$$\rho = 1.02 \pm 0.06 \qquad (18)$$

in good agreement with the minimal SU(2)⊗U(1) model.

ACKNOWLEDGEMENTS

This experiment would have been impossible without the collective effort of the staffs and coordinators of all accelerators involved in the CERN $\bar{p}p$ Collider, whom we gratefully acknowledge.

We are grateful to F. James for illuminating discussions on the statistical analysis of samples consisting of a small number of events.

We deeply thank the technical staffs of the institutes collaborating in UA2 for their important contributions.

Financial supports from the Schweizerischer Nationalfonds zur Förderung der Wissenschaftlichen Forschung to the Bern group, from the Danish Natural Science Research Council to the Niels Bohr Institute group, from the Institut National de Physique Nucléaire et de Physique des Particules to the Orsay group, from the Istituto Nazionale di Fisica Nucleare to the Pavia group and from the Institut de Recherche Fondamentale (CEA) to the Saclay group are acknowledged.

REFERENCES

1. M. Banner et al., Phys. Lett. 122B (1983) 476.

2. S.L. Glashow, Nucl. Phys. 22 (1961) 579.
   S. Weinberg, Phys. Rev. Lett. 19 (1967) 1264.
   A. Salam, Proc. 8th Nobel Symposium, Aspenäsgården, 1968 (Almqvist and Wiksell, Stockholm), p. 367.

3. P. Bagnaia et al., Phys. Lett. 129B (1983) 130.

4. For a review see J. Ellis et al., Ann. Rev. Nucl. Part. Science 32 (1982) 443.

5. The UA2 Collaboration, Latest results from the UA2 experiment at the CERN $\bar{p}p$ Collider, Proc. of the Int. Europhysics Conf. on High Energy Physics, Brighton, July 1983, p. 472.

6. A.G. Clark, Results from the UA2 experiment at the CERN $\bar{p}p$ Collider, Proc. of the 1983 Int. Symp. on Lepton and Photon Interactions at High Energies, Cornell, August 1983, p. 53.

7. B. Mansoulié, The UA2 apparatus at the CERN $\bar{p}p$ Collider, Proc. of the 3rd Moriond Workshop on $\bar{p}p$ physics (1983) p. 609 (éditions Frontières).

8. M. Dialinas et al., The vertex detector of the UA2 experiments, LAL-RT/83-14 (1983).

9. A. Beer et al., The central calorimeter of the UA2 experiment at the CERN $\bar{p}p$ Collider, CERN-EP/83-175 (1983) to be published in Nucl. Instr. Meth.

10. M. Banner et al., Phys. Lett. 115B (1982) 59.

11. M. Banner et al., Phys. Lett. 122B (1983) 322.

12. C. Conta et al., The system of forward-backward drift chambers in the UA2 detector, CERN-EP/83-176 (1983) to be published in Nucl. Instr. Meth.

13. K. Borer et al., Multitube proportional chambers for the localization of electromagnetic showers in the UA2 detector, CERN-EP/83-177 (1983) to be published in Nucl. Instr. Meth.

14. R. Battiston et al., Phys. Lett. 117B (1982) 126.
G. Sanguinetti, Proc. of the 3rd Moriond Workshop on $\bar{p}p$ physics (1983) p. 25 (éditions Frontières).

15. P. Bagnaia et al., Z. Phys. C20 (1983) 117.

16. P. Bagnaia et al., Measurement of very large transverse momentum jet production at the CERN $\bar{p}p$ Collider, CERN-EP/84-12 (1984) to be published in Phys. Lett. B.

17. G. Altarelli, R.K. Ellis, M. Greco and G. Martinelli, Vector boson production at Colliders : a theoretical reappraisal, Ref. TH. 3851-CERN (1984).
For earlier calculations see:
E.L. Berger, Proc. AIP Conf. on New Results in High Energy Physics, Vanderbilt University (1978), p. 178, R.S. Panvini and S.E. Coorna editors (American Institute of Physics, New York, 1978).
F. Halzen and W. Scott, Phys. Lett. 78B (1978) 318.
P. Chiappetta and M. Greco, Transverse momentum distributions for weak bosons at the $p\bar{p}$ Collider, Frascati report LNF-83/44 Rev., October 1983.
A. Nakamura, G. Pancheri and Y. Srivastava, Frascati report LNF-83/43(R), June 1983.
P. Aurenche and J. Lindfors, Nucl. Phys. B185 (1981) 274.

18. P. Bagnaia et al., Observation of electrons produced in association with hard jets and large missing tansverse momentum in $p\bar{p}$ collisions at $\sqrt{s}$ = 540 GeV, CERN-EP/84-40, submitted to Phys. Lett. B.

19. M. Glück et al., Z. Phys. C13 (1982) 119.

20. G. Arnison et al., Phys. Lett. 129B (1983) 273.

21. F.E. Paige and S.D. Protopopescu, BNL report 31987 (1981).

22. Review of Particle Properties, Phys. Lett. 111B (1982).

23. P. Minkowski, Remarks on W production in $\bar{p}p$ collisions at $\sqrt{s}$ = 540 GeV, University of Bern preprint BUTP-83/22 (1984) to be published in Phys. Lett. B.

24. G. Arnison et al., Phys. Lett. 126B (1983) 398.
B. Sadoulet, Experimental observation of lepton pairs of invariant mass around 95 GeV/c^2 at the CERN $p\bar{p}$ Collider, Proc. of the 1983 Int. Symp. on Lepton and Photon Interactions at High Energies, Cornell, August 1983, p. 27.

25. B. Humpert and W.L. van Neerven, Phys. Lett. 93B (1980) 456.

26. C. Jarlskog and F.J. Yndurain, Phys. Lett. 102B (1983) 361.
F. Halzen and K. Mursula, Limits to the number of neutrinos, a comment on Z^0 discovery, University of Helsinki preprint HU-TFT)83-36 (1983).
K. Hikasa, Counting neutrino species at high-energy proton-antiproton collisions, University of Wisconsin preprint MAD/PH/144 (Nov. 1983).

27. D. Albert, W.J. Marciano, D. Wyler and Z. Parsa, Nucl. Phys. B166 (1980) 460.
F. A. Berends and R. Kleiss, Hard Photon Effects in $W^{\pm}$ and Z^0 decay, University of Leiden, The Netherlands, Nov. 1983.

28. See, for example, E.J. Dudewicz, Introduction to Statistics and Probability (1976) p. 277 (edited by Holt, Rinehart and Winston, New York).

29. W.T. Eadie et al., Statistical methods in experimental physics (1971) p.282 (edited by North-Holland, Amsterdam). We thank B.Sadoulet for making us aware of this technique.

30. G. Arnison et al., Phys. Lett. 135B (1984) 250.

31. The observation of $Z^0 \to \ell^+\ell^-\gamma$ decays has prompted several theoretical speculations. See for example:
M.J. Duncan and M. Veltman, Validity of Standard Model at 90 Gev, University of Michigan report UM TH 84-1 (1984).
M. Veltman, Bound States of Vector Bosons, University of Michigan report UM-HE 83-22, December 1983.
F.M. Renard, Interpretations of $Z^0 \to e^+e^-\gamma$ events and additional tests, University of Montpellier report PM/83/11, December 1983.
L. Bergström, Note on the anomalous Z^0 decays, Royal Institute of Technology report TRITA-TFY-83/29, Stockholm, December 1983.
A. De Rujula, L. Maiani and R. Petronzio, Search for excited quarks, CERN-TH 3779 (1983).
G. Passarino, Phys. Lett. 130B (1983) 115.
T.G. Rizzo, High energy photons as probes of the internal structure of the Z^0 boson, Iowa State University report IS-J 1238 (1983).
N. Cabibbo, L. Maiani and Y. Srivastava, Anomalous Z^0 decays: excited leptons?, University of Rome report no. 381, November 1983.
G. Gounaris, R. Kögerler and D. Schildknecht, On $Z^0 \to e^+e^-\gamma$ decays, University of Bielefeld report BI-TP 83/17 (1983).

32. For a review see W.J. Marciano, Electroweak interactions, Proc. of the 1983 Int. Symp. on Lepton and Photon Interactions at High Energies, Cornell, August 1983, p. 80.
Early calculations can be found in:
W.J. Marciano, Phys. Rev. D20 (1979) 274.
F. Antonelli, M. Consoli and G. Corbò, Phys. Lett. 91B (1980) 90.
M. Veltman, Phys. Lett. 91B (1980) 95.

F. Antonelli, M. Consoli, G. Corbò and O. Pellegrino, Nucl. Phys. B183 (1981) 195.
F. Antonelli and L. Maiani, Nucl. Phys. B186 (1981) 269.
M. Consoli, S. Lo Presti and L. Maiani, Higher order effects and the vector boson physical parameters, University of Catania report PP/738, 14 January 1983.

33. A. Sirlin, Phys. Rev. D22 (1980) 971.
W.J. Marciano and A. Sirlin, Phys. Rev. D22 (1980) 2695.

34. A. Sirlin and W.J. Marciano, Nucl. Phys. B189 (1981) 442.
C. Llewellyn Smith and J. Wheater, Phys. Lett. 105B (1981) 486.

Table I - Electron identification criteria

a) Central detector

Physical quantity	Description	Cuts	Efficiency η (isolated electron)
Calorimeter energy	Radius R_θ, R_ϕ	$R_\theta, R_\phi < 0.5$ cells	1.0
	Hadronic leakage $E_{had}/E_{cl} < H_0$	$H_0 = 0.035 + 0.051 \ln E_{cl}$ *)	0.99
Associated track	Distance Δ between track and cluster centroid. At least one hit in chambers C_1 or C_2.	$\Delta < 1$	0.90
Preshower signal**)	Signal from chamber C_5 within distance d_0 from track intercept.	$d_0 = 7$ mm*)	0.95
	Associated charge $Q_5 > Q_0$	$Q_0 \approx 3$ m.i.p.	0.95
	No additional cluster within distance d_1 of selected cluster, with charge larger than Q_5	$d_1 = 60$ mm	1.0
Track-energy cluster match	Require energy pattern to agree with that expected from electron : $P(\chi^2) > P_0$	$P_0 = 10^{-4}$**)	0.95
		Overall efficiency	0.76 ± 0.05

*) Strict cuts : $H_0 = 0.023 \pm 0.034 \ln E_{cl}$ ($\eta = 0.95$)
$d_0 = 5.5$ mm ($\eta = 0.90$)
$P_0 = 10^{-2}$ ($\eta = 0.90$)

**) This cut is not applied in a region $\Delta\phi = 18^\circ$ wide where chamber C_5 was not operational.

b) Forward detectors

Physical quantity	Description	Cuts	Efficiency (isolated electrons)
Calorimeter energy	Cluster size $\leq$ 2 cells Energy fraction (charged and neutral) in adjacent cells $< f_0$	$f_0 = 0.05$	1.0
	Energy leakage $E_{leak}/E_{em} < H_0$	$H_0 = 0.02$ *)	0.99
Associated track	Forward track crossing cluster cell. Track minimum distance t from vertex in transverse projection less than t_0	t_0 = 20 mm	0.98
	Associated transverse vertex track within $\|\Delta\phi\| < \phi_0$ At least one hit in chambers C_1 or C_2. No identified conversion	ϕ_0 = 30 mr	0.96
Preshower signal	Signal in each MTPC plane within distance δ_0 of track intercept : $\|\Delta x\| < \delta_0$, $\|\Delta y\| < \delta_0$	δ_0 = 20 mm	0.99
	Associated MTPC charge $Q > Q_0$	$Q_0 \approx$ 6 m.i.p.	0.93
Preshower-energy cluster match	Distance of projected MTPC position and cluster centroid as evaluated from PM ratio $\|\Delta x\| < \Delta_0$	Δ_0 = 100 mm	0.98
Momentum	Momentum p and calorimeter energy E satisfy $\|p^{-1}-E^{-1}\|/\sigma(p^{-1}-E^{-1})<\alpha_0$	$\alpha_0 = 4$	0.95 **)
		Overall efficiency	0.80 ± 0.05

*) A cut $H_0 = 0.03$ is applied if the energy is shared between two adjacent cells.

**) This value takes into account both internal and external bremsstrahlung.

Table II

a) Numbers of events containing an electron candidate with $p_T^e > 15$ GeV/c (after removal of the eight Z^o events [3])

Topology	Central detector	Forward detectors
No additional jets	38	7
Jets with $\rho_{opp} < 0.2$	20	4
Jets with $\rho_{opp} > 0.2$	135	13

b) Numbers of $W \to e\nu$ candidates with $P_T^e > 25$ GeV/c and background estimates

	Central detector	Forward detector
Signal	30	7
Background	1.4 ± 0.1	0.05

Table III

a) Parameters of the Z^o events

Event	A	B	C	D	E	F	G	H
E_1(GeV)	71.5±1.8	48.4±1.7	69.9±1.8	104.5±6.4	60.0±2.0	55.6±2.1	45.1±1.5	46.3±1.6
E_2(GeV)	49.7±1.6	72.1±2.6	11.5±0.7	51.3±1.6	38.6±1.4	46.6±1.6	47.6±1.5	42.1±1.4
k (GeV)			24.4±1.0					
M(GeV/c^2)	91.6±1.9	94.6±2.4	90.6±1.9	91.9±3.2	95.5±2.3	92.0±2.3	83.4±1.9	88.0±2.1
p_T(GeV/c)	0.4±1.4	12.7±1.8	1.4±0.6	2.7±1.7	6.2±1.1	5.5±2.0	10.4±1.8	6.7±0.9

Other relevant parameters are given in Ref. 3

b) Parameters of event C ($Z^o \to e^+e^-\gamma$) in the Z^o rest frame

$2E(e^+)/M_Z$	0.989	$M(e^+e^-)$ GeV/c^2	50.4±1.7
$2E(e^-)/M_Z$	0.318	$M(e^-\gamma)$ GeV/c^2	9.1±0.3
$2k/M_Z$	0.690	$M(e^+\gamma)$ GeV/c^2	74.7±1.8
$\omega(e^-\gamma)$(deg.)	$25^o \pm 1^o$		

FIGURE CAPTIONS

1. A view of the UA2 detector in a plane containing the beam line.

2. Exploded view of a sector in one of the two forward regions.

3. Transverse momentum distribution of the 227 electron candidates satisfying the selection criteria of Table I.

4. a) Transverse momentum distribution of the electron candidates in events with no additional jets.
   b) Transverse momentum distribution of the electron candidates in events with additional jets having $\rho_{opp} > 0.2$ (see Eq. 3). The dark area corresponds to the eight Z^0 events for which only the electron with the higher p_T^e is plotted.
   c) Transverse momentum distribution of the electron candidates in events with additional jets having $\rho_{opp} < 0.2$.
   The curves represent the background estimates as discussed in Section 6.

5. a) Distribution of the azimuthal separation $\Delta\phi$ between the momentum vector of the electron candidate and that of the associated jet having the highest p_T.
   b) Distribution of ρ_{opp} (see Eq. 3) for events containing an electron candidate and at least one associated jet.
   The curves represent the background estimates as discussed in Section 6.

6. a) Transverse momentum distributions of the electron candidate in the $W \rightarrow e\nu$ event sample; b) strict cuts applied in the central detector.
   Full curves : background estimates as discussed in Section 6.
   Dashed curve : the sum of all expected contributions as discussed in Section 10.

7. Quality parameters of the electron candidates with $p_T^e > 25$ GeV/c in the $W \rightarrow e\nu$ sample. Central detector : a) distribution of the ratio E_{had}/E_{cl} normalised to the value of H_0 used in the strict cuts (see Table Ia) ; b) distribution of d^2 ; c) distribution of Q_s. Forward detectors : d) distribution of the ratio E_{leak}/E_{em} ; e) scatter plot of the signal position in the preshower counter with respect to the track impact point ; f) distribution of Q(MTPC) ; g) Distribution of the most likely ionisation I_0 associated with the electron candidate track (full histogram). The dashed histogram is the corresponding distribution for tracks in minimum bias events.

8. a) Uncorrected distribution of the W transverse momentum (from Eq. 5 with $\lambda = 1$).
b) Corrected distribution (from Eq. 5 with $\lambda = 2.2$). The curve represents a QCD prediction [17].

9. Scatter plots of the 69 $W \rightarrow e\nu$ candidates : a) in the plane p_T^e, p_ξ^e ; b) in the plane p_T^e, p_η^ν.

10. Plot of 1/E vs $1/\hat{p}$ for the eight $W \rightarrow e\nu$ candidates with $p_T^e > 20$ GeV/c detected in the forward regions. The quantity $\hat{p}$ is the product of the electron momentum, as measured by magnetic deflection, with the sign of the product $q\cos\theta_e$ where $q = +1$ (-1) for $e^+(e^-)$.

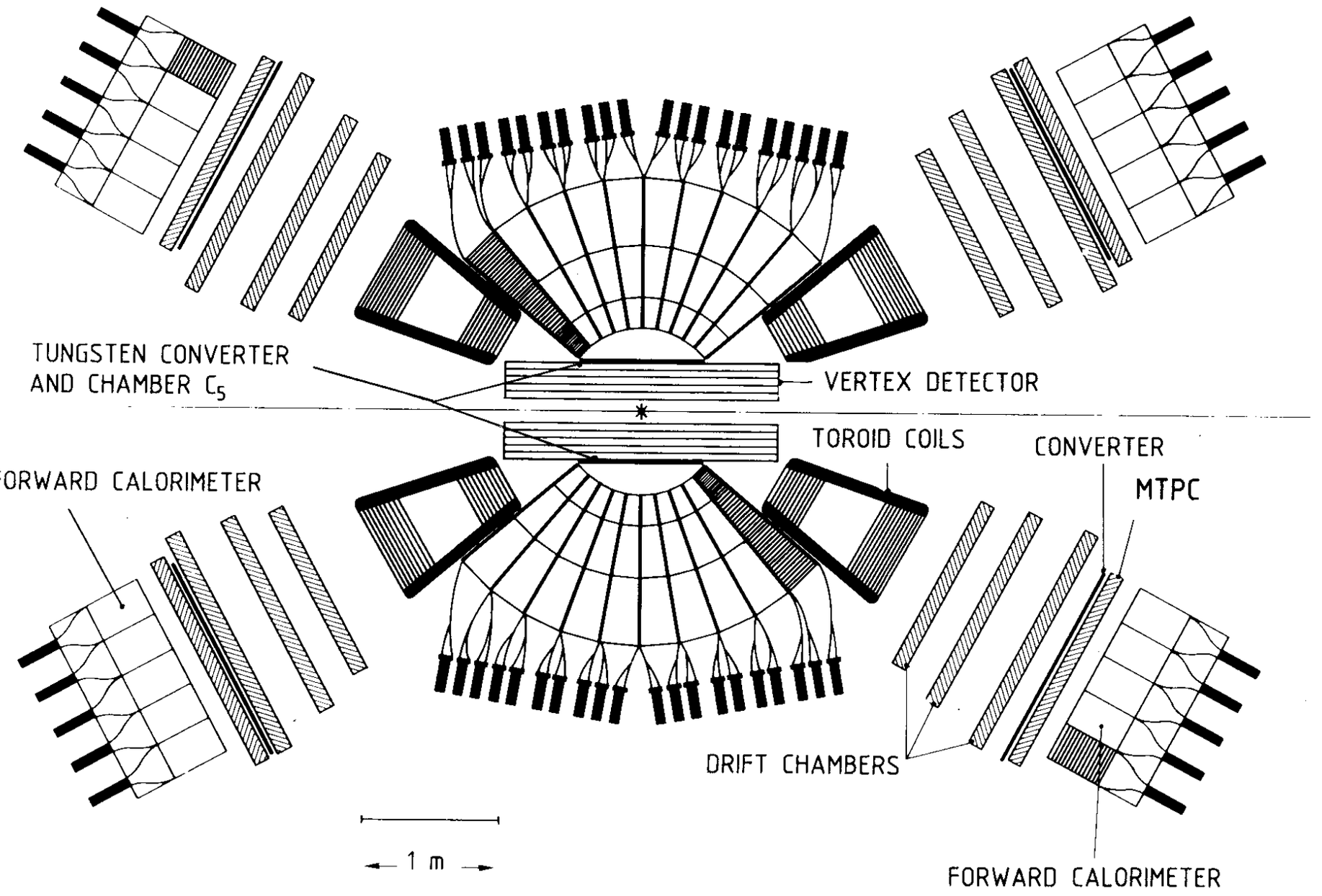
TUNGSTEN CONVERTER
AND CHAMBER C_5
VERTEX DETECTOR
TOROID COILS
CONVERTER
MTPC
FORWARD CALORIMETER
DRIFT CHAMBERS
1 m
FORWARD CALORIMETER

Fig. 1

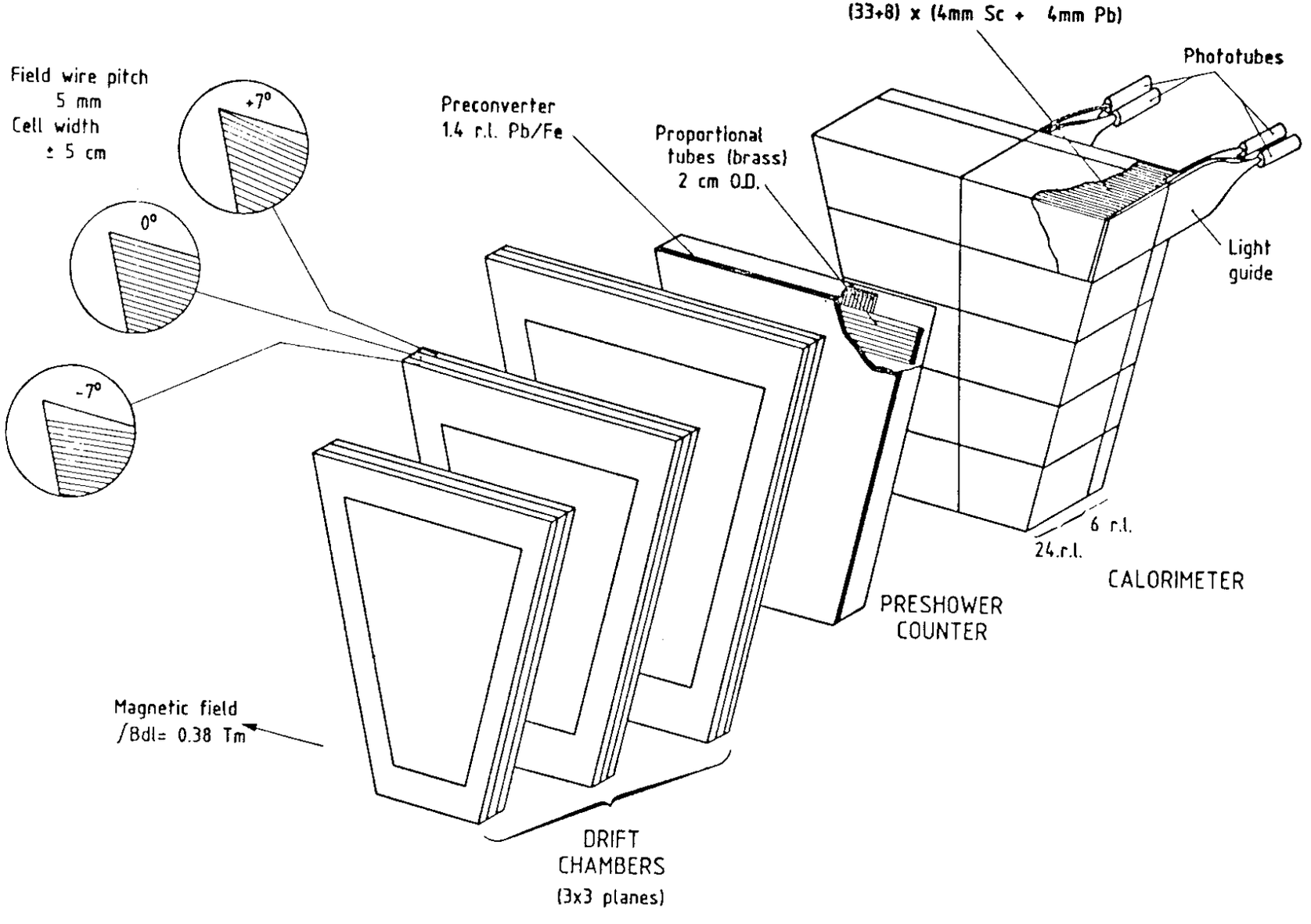
(33+8) x (4mm Sc + 4mm Pb)
Phototubes
Field wire pitch
5 mm
Cell width
± 5 cm
+7°
0°
-7°
Preconverter
1.4 r.l. Pb/Fe
Proportional
tubes (brass)
2 cm O.D.
Light
guide
6 r.l.
24 r.l.
CALORIMETER
PRESHOWER
COUNTER
Magnetic field
/Bdl= 0.38 Tm
DRIFT
CHAMBERS
(3x3 planes)

Fig. 2

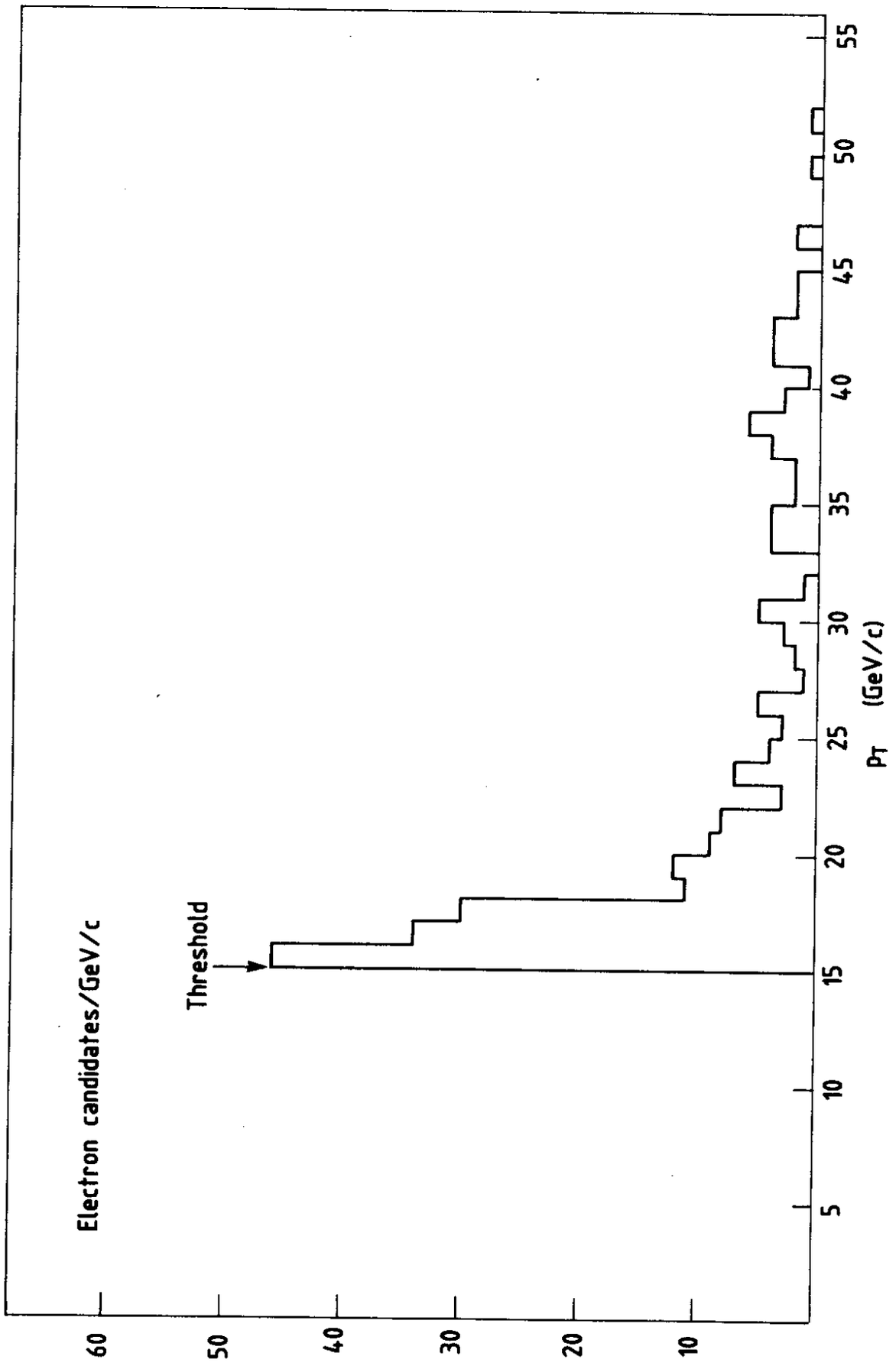
Electron candidates/GeV/c
Threshold
p_T (GeV/c)
60
50
40
30
20
10
5
10
15
20
25
30
35
40
45
50
55

Fig. 3

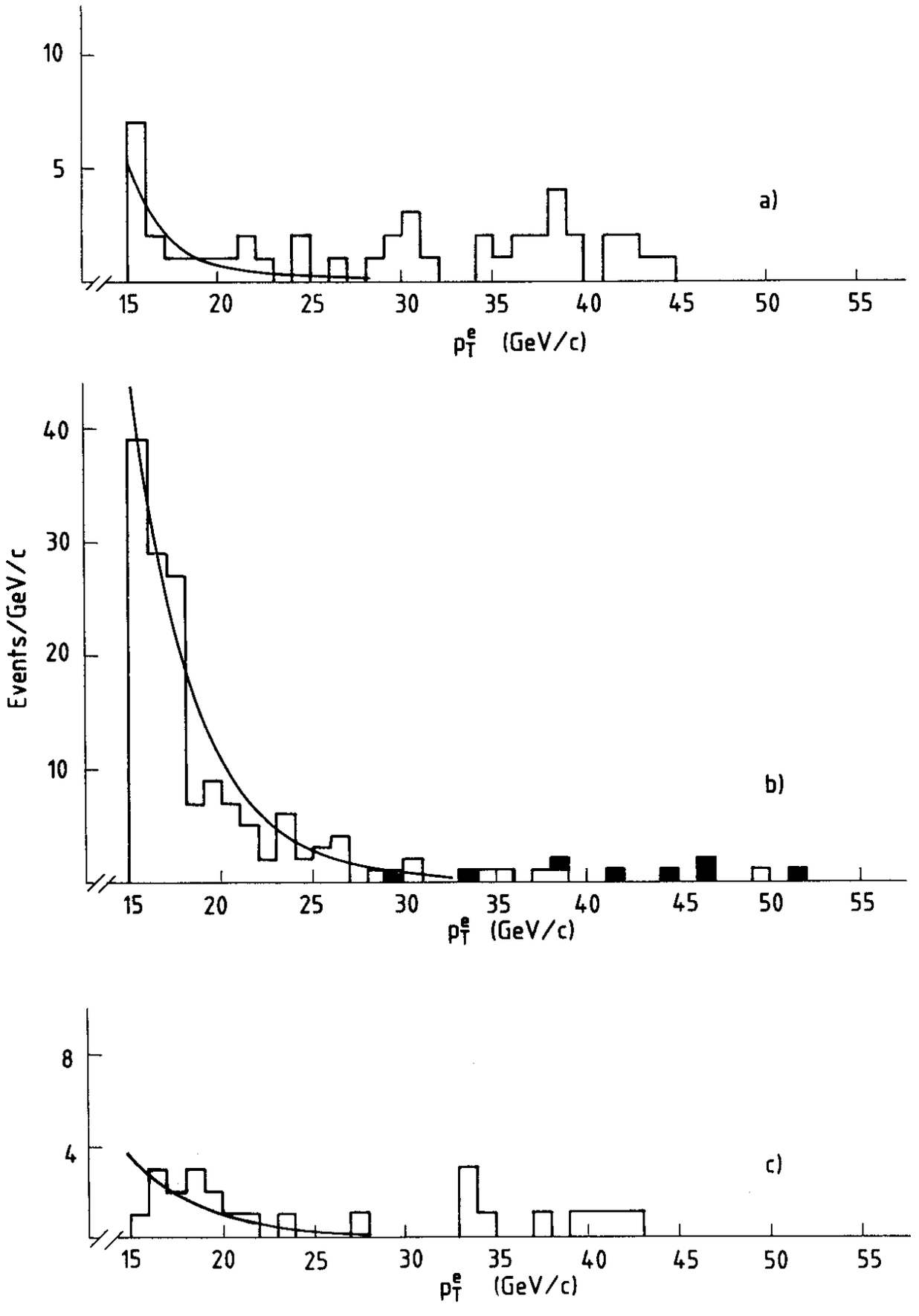
10
5
a)
15
20
25
30
35
40
45
50
55
p_T^e (GeV/c)
40
30
20
10
Events/GeV/c
b)
15
20
25
30
35
40
45
50
55
p_T^e (GeV/c)
8
4
c)
15
20
25
30
35
40
45
50
55
p_T^e (GeV/c)

Fig. 4

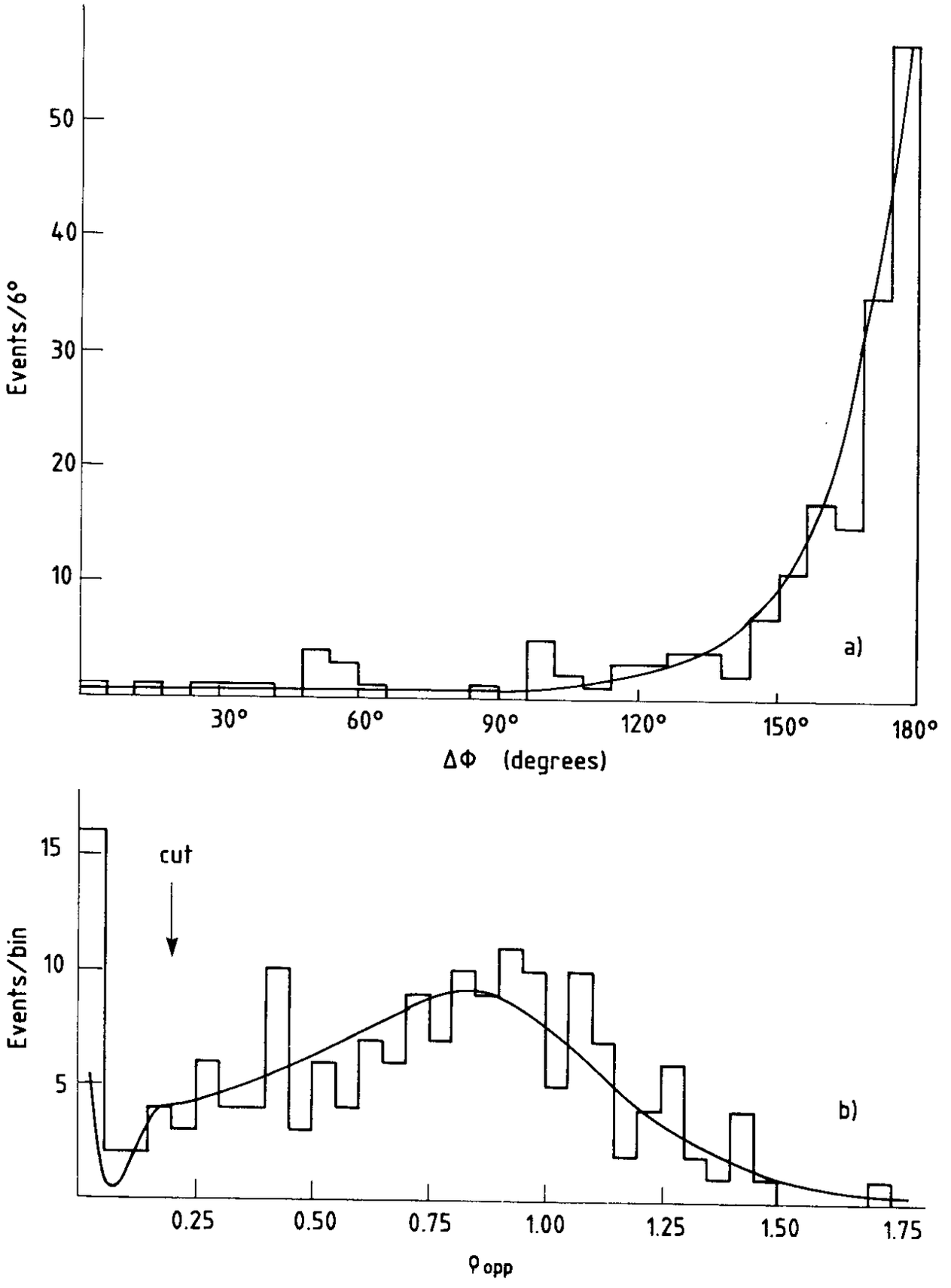
50
40
30
20
10
Events/6°
a)
30°
60°
90°
120°
150°
180°
ΔΦ (degrees)
15
10
5
Events/bin
cut
b)
0.25
0.50
0.75
1.00
1.25
1.50
1.75
ρopp

Fig. 5

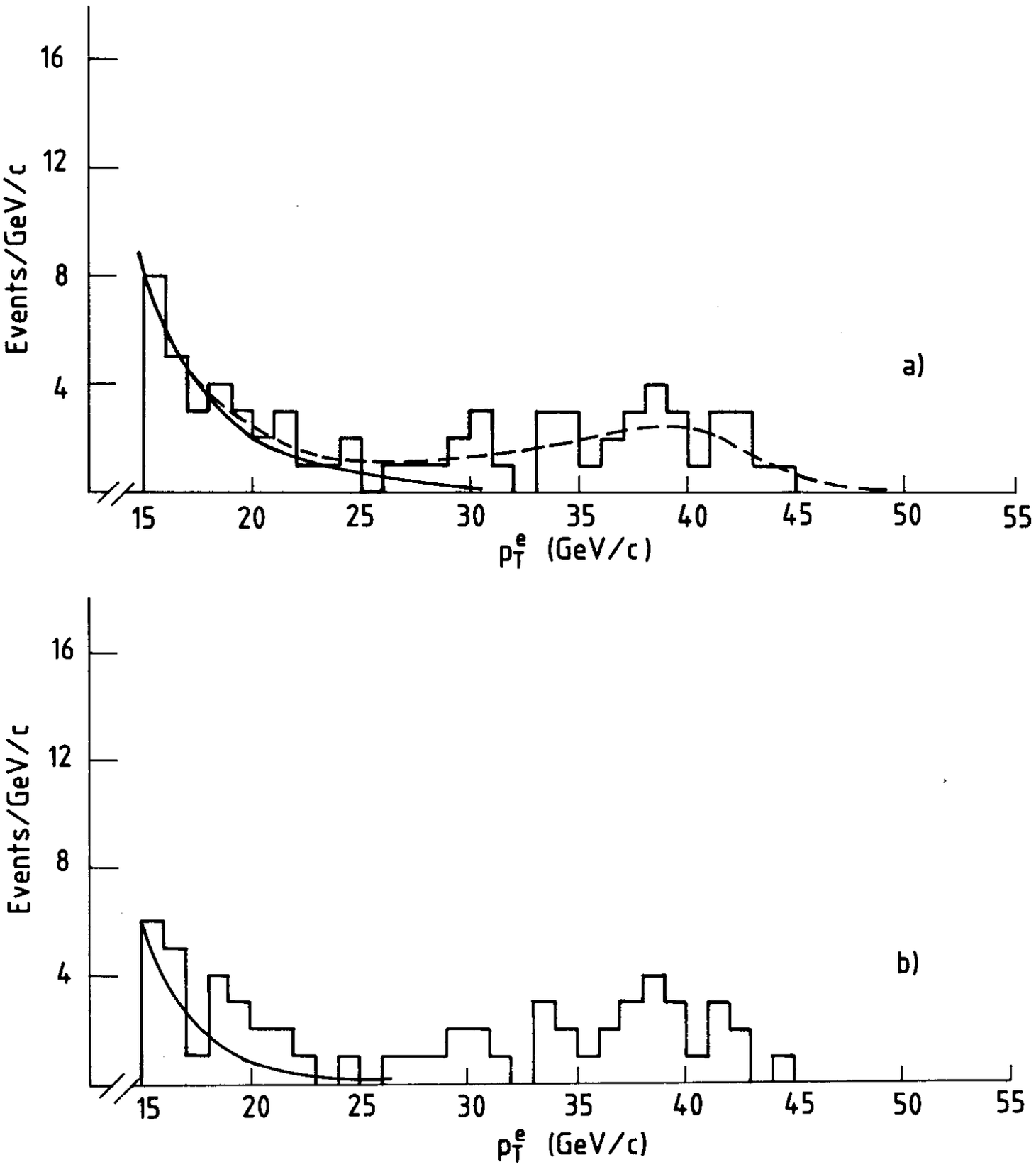
16
12
8
4
Events/GeV/c
a)
15
20
25
30
35
40
45
50
55
p_T^e (GeV/c)
16
12
8
4
Events/GeV/c
b)
15
20
25
30
35
40
45
50
55
p_T^e (GeV/c)

Fig. 6

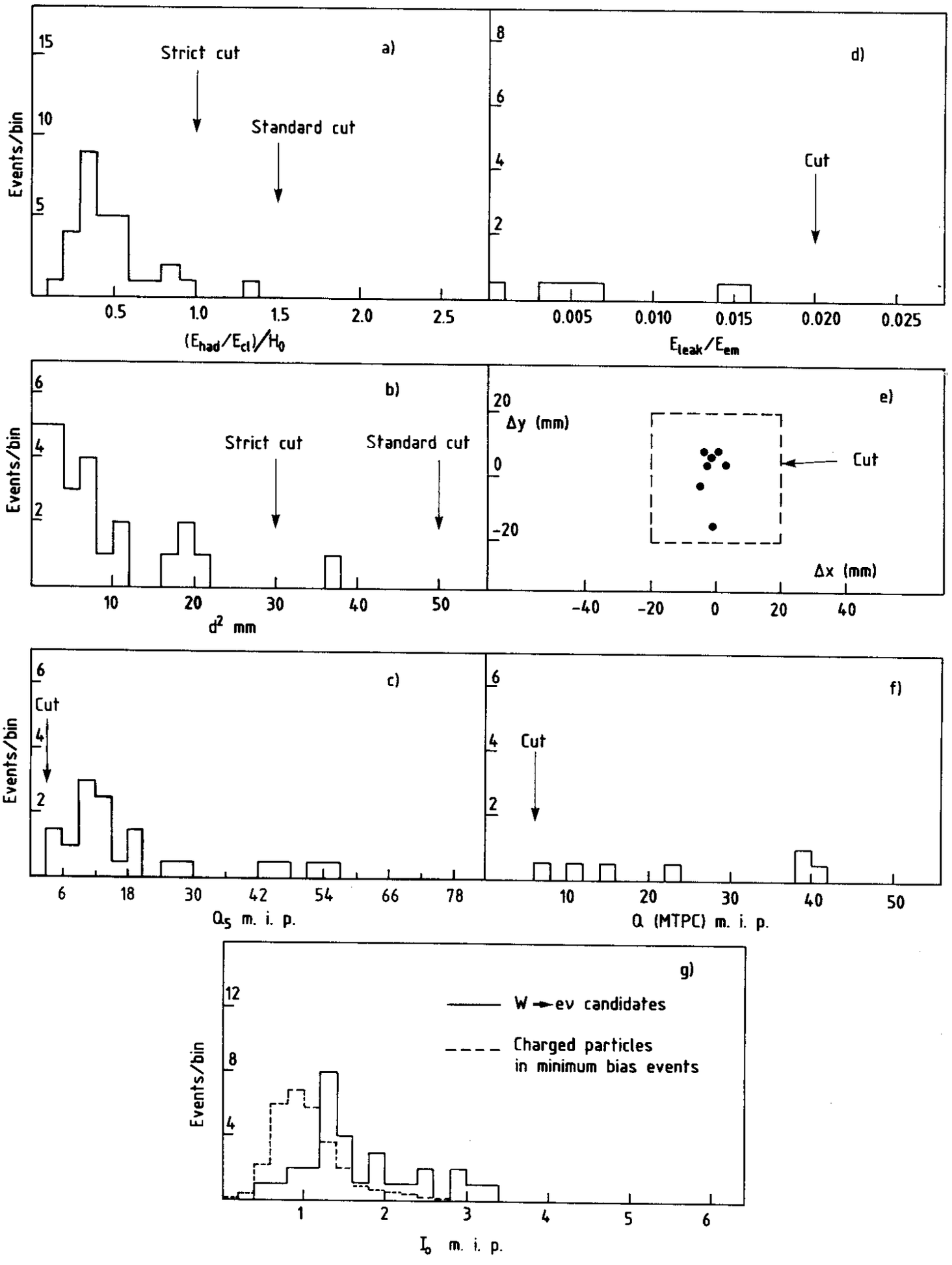
a)
Strict cut
Standard cut
Events/bin
$(E_{had}/E_{cl})/H_0$
d)
Cut
E_{leak}/E_{em}
b)
Strict cut
Standard cut
d^2 mm
e)
Δy (mm)
Cut
Δx (mm)
c)
Cut
Q_S m. i. p.
f)
Cut
Q (MTPC) m. i. p.
g)
W → eν candidates
Charged particles in minimum bias events
I_0 m. i. p.

Fig. 7

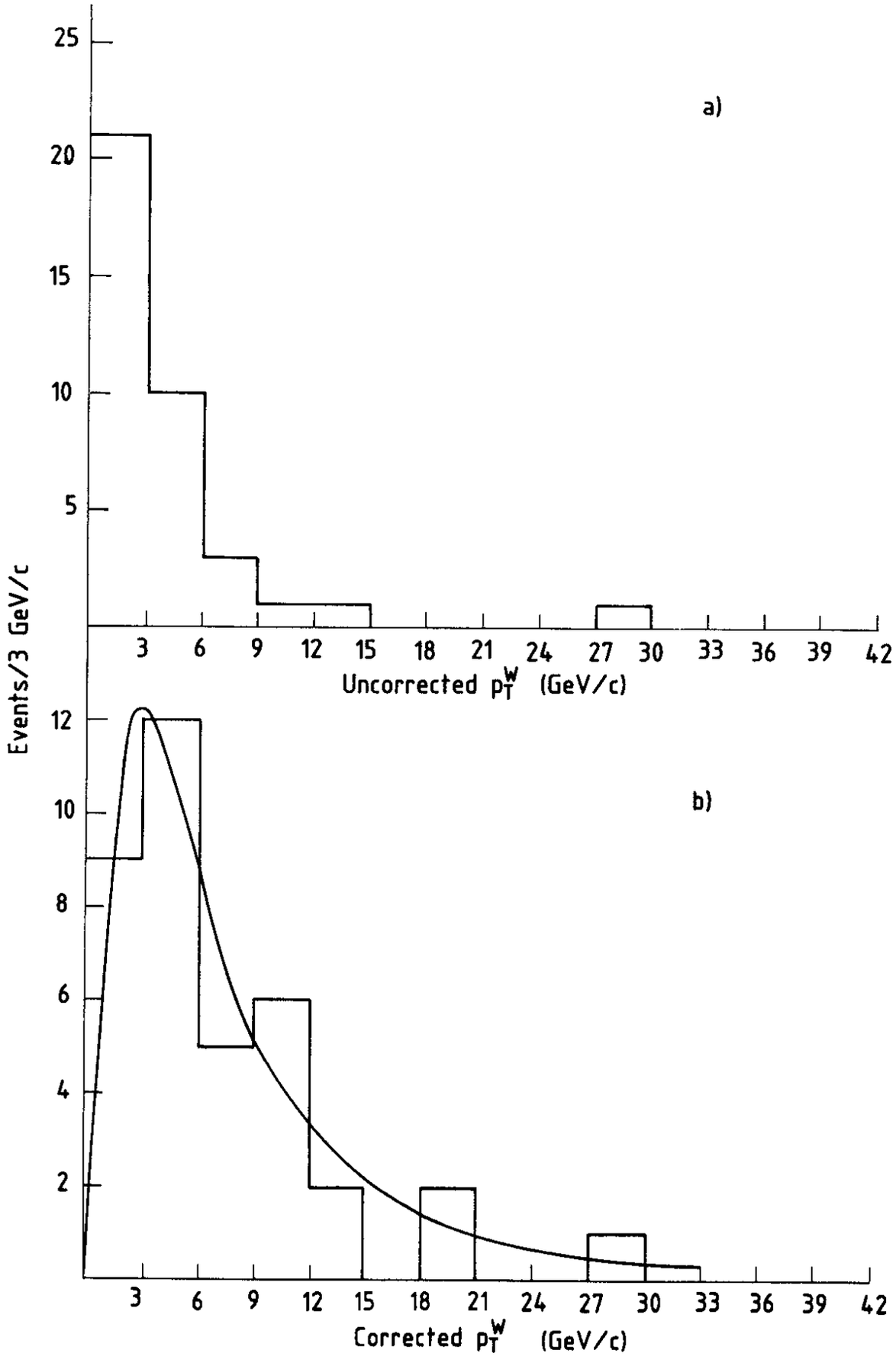
a)
b)
Events/3 GeV/c
Uncorrected p_T^W (GeV/c)
Corrected p_T^W (GeV/c)
25
20
15
10
5
12
10
8
6
4
2
3
6
9
12
15
18
21
24
27
30
33
36
39
42

Fig. 8

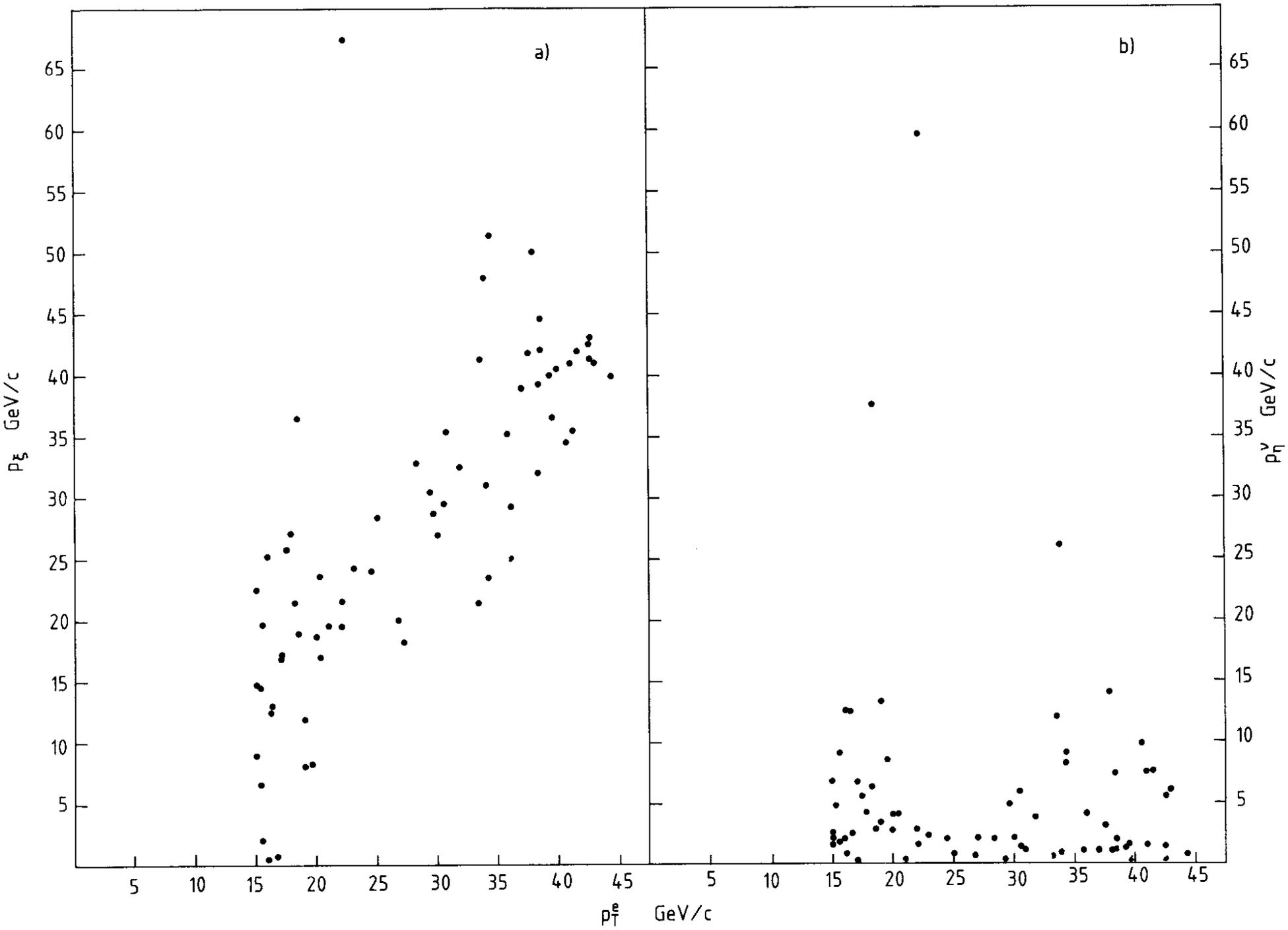
a)
b)
p_ξ GeV/c
p_η^ν GeV/c
p_T^e GeV/c
5
10
15
20
25
30
35
40
45
50
55
60
65

Fig. 9

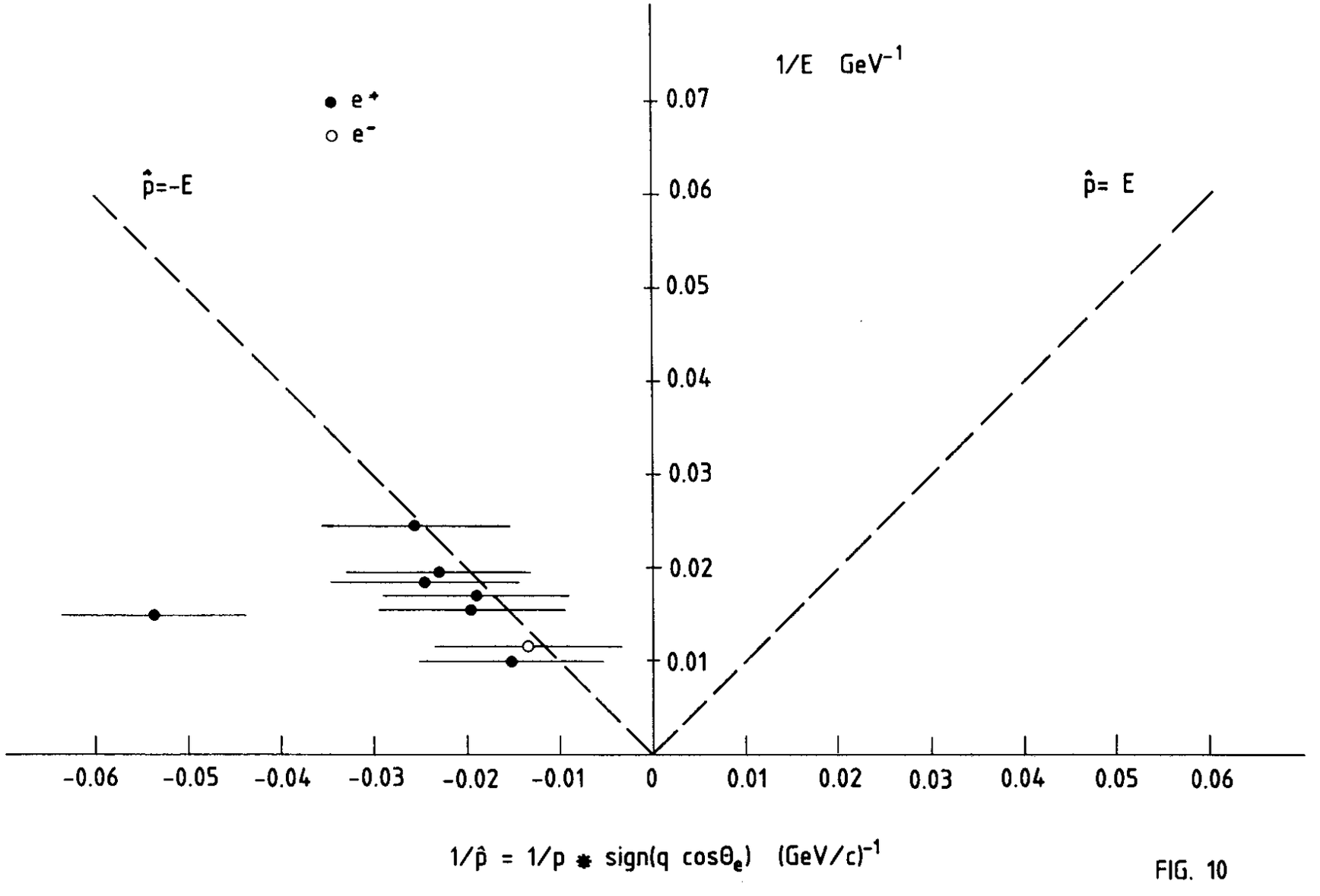
1/E GeV^{-1}
● e$^+$
○ e$^-$
$\hat{p}$=-E
$\hat{p}$= E
0.07
0.06
0.05
0.04
0.03
0.02
0.01
-0.06
-0.05
-0.04
-0.03
-0.02
-0.01
0
0.01
0.02
0.03
0.04
0.05
0.06
$1/\hat{p} = 1/p * \mathrm{sign}(q \cos\theta_e)$ (GeV/c)$^{-1}$

Fig. 10

FIG. 10